Thesis, COLLÉGIALITÉ, FRANZEN Rachelle

Auteur : Pereira Da Cunha, Liliana
Promoteur(s) : Sandersen, Charlotte; Franck, Thierry
Faculté : Faculté de Médecine
Diplôme : Master en sciences biomédicales, à finalité approfondie
Année académique : 2024-2025
URI/URL : http://hdl.handle.net/2268.2/23204

Can primary human Muscle-derived stem-cells (hMuSCs) recover or mitigate mitochondrial dysfunction in skeletal muscle tissue?

Establishment of a model for mitochondrial dysfunction using an exogenous H_2O_2-stress on the LHCN-M2 cell line

Pereira Da Cunha Liliana Filipa
2024/2025
Centre de l'Oxygène, Recherche et développement (CORD)
ULiege

Thesis for the obtention of a multidisciplinary master degree in Biomedical sciences in english

Dr Franck Thierry
P Sandersen Charline

University of Liege

Acknowledgements

Je tiens à exprimer ma profonde gratitude à mon promoteur, Thierry Franck, pour son accompagnement rigoureux, sa bienveillance et, surtout, pour toute la patience dont il a fait preuve face à ma lenteur parfois désarmante.
Un immense merci à Ariane Niesten pour toute sa pédagogie, sa douceur constante et pour m'avoir transmis des compétences précieuses, surtout en culture cellulaire.
Ma reconnaissance va également à Ange Mouithys-Mickalad et à Madame Deby pour toutes nos échanges enrichissants lors des pauses de midi; vos conversations ont grandement contribué à élargir ma culture générale.
Je me considère extrêmement chanceuse d'avoir pu intégrer un laboratoire aussi chaleureux et stimulant, entourée de professionnels passionnés.
Je tiens encore à remercier tous les responsables de l'équipe CORD et RevaTis, le Professeur Didier Serteyn, le Professeur Charline Sandersen et le Dr Justine Ceusters, pour m'avoir donné l'opportunité d'explorer un sujet qui, à mes yeux, représente une voie d'avenir majeure en recherche biomédicale fondamentale et clinique.
Un merci tout particulier à Gaëtan Lefèvre de l'équipe de Giga-Cell imaging pour son soutien technique et pour sa disponibilité précieuse lors de l'utilisation du système IncuCyte.

A ma famille et à mes amis, plus spécialement à mon Steve, merci pour votre soutien indéfectible, les encouragements et soutien moral inébranlable tout au long de mes études et de mes coups de tête.

Enfin, ce mémoire n'aurait probablement jamais vu le jour sans mon frère, Rafael. Si un jour j'ai la chance de tracer une petite carrière dans le monde de la recherche mitochondriale et du métabolisme musculaire, ce sera pour toi.

Table of contents

Introduction

Project context: brief presentation of the MitoSir project....1

Skeletal Muscle tissue....2

Mitochondria....4

Structure and Function....4

Krebs Cycle and Electron Transport Chain (ETC)....6

Reactive species (RS) and oxidative stress (OS)....7

Mitochondrial dysfunction in aging and disease....9

Types of in vitro models....10

Exogenous H_2O_2 treatment....10

Analysis of mitochondrial function....12

MTS and CellTiter-Glo assays....12

High-Resolution Respirometry (HRR)....13

Principle....13

Protocol for living cells....13

Data treatment and interpretation....15

Hypothesis and strategies....15

Materials & Methods....16

Results

Development of a standardized exogenous H_2O_2 stress....25

Effect of H_2O_2 dilution in culture medium or HBSS....25

Effect of the initial seeding....25

Effect of the incubation time....26

Effect of the exogenous H2O2 treatment on cellular viability....27

Transposition of the stress protocol to larger culture formats....28

Effect of the exogenous H_2O_2 treatment on mitochondrial function....31

High-Resolution respirometry (HRR)....31

Citrate synthase activity....33

ROS analysis using H_2DCFda probe....34

Discussion, Conclusions, prospectives....35

References....41

Abbreviations

AA: Antimycin A

ETC: Electron Transport Chain

ETSmax: Electron Transport System maximum

H_2DCFda: 2'-7'-Dichlorodihydrofluorescein diacetate (ROS assay)

FCCP: CarbonylCyanide-P-TriFluomethoxyphenylhydrazone

FCR: Flux Control Ratio

FGF2: Fibroblast Growth Factor 2

GPx: Glutathione Peroxidase

H2O2: Hydrogen peroxide

HGF: Hepatic Growth Factor

HRR: High-Resolution Respirometry

IMM: Inner Mitochondrial Membrane

IMS: InterMembrane Space

LHCN-M2: Immortalized Human muscle-derived myoblast cell line

mtDNA: mitochondrial DNA

MTS: 3-(4,5-dimethylthiazol-2-yl9-5-(3-carboxymethoxyphenyl)-2-(4-sulfophenyl)-2H-tetrazolium

nDNA: nuclear DNA

OCR: Oxygen Consumtion Rate

OMM: outer Mitochondrial Membrane

OS: Oxidative stress

OXPHOS: Oxidative Phosphorylation

PEM: Phenazine MethoSulfate

PES: Phenazine EthoSulfate

ROS: Reactive Oxygen Species

RS: Reactive Species

TCA: TriCarboxylic Acid Cycle

TRx: ThioRedoxin

Summary

Sarcopenia is a geriatic syndrome characterized by an age-related progressive loss of muscle mass and strength, which carries multiple personal, economic and social burdens.
With the ever so growing improvements in the healthcare system and in the lifestyle conditions, its incidence is expected to rise in the upcoming years.

Although the etiologic context of this syndrome is vastly heterogeneous, recent studies have highlighted the role of mitochondria and mitochondrial dysfunction in its onset. Skeletal muscle—a high metabolically active tissue that is especially vulnerable to mitochondrial dysregulations. Slight alterations in the mitochondrial function can lead to significant clinical manifestations.

This study was conducted within the framework of a Wallonia Region financed collaborative R&D project called MitoSir, which brings together multiple research partners— including ULiege (CORD), RevaTis SA., GenFlow Bioscience and ULB— to explore potential of stem cells as a therapeutic strategy to sarcopenia .

In this study, we used an immortalized human myoblast cell line (LHCN-M2) and an exogenous hydrogen peroxide (H_2O_2) treatment on adherent LHCN-M2 cells to simulate an oxidative environment potentially inductive of a mitochondrial dysfunction, two hallmarks of sarcopenia.

Our High-Resolution Respirometry (HRR) results showed that the exogenous H_2O_2 treatment increases mitochondrial leak respiration in a time- and dose-dependent manner. ETS_{max} showed a tendency to decrease. Finally, results from the CellTiter-Glo assay, used to evaluate cellular ATP content, corroborate these findings, showing a dose-dependent collapse in ATP levels following H_2O_2 treatment without inducing cell mortality.
Globally speaking, our results point towards a mitochondrial dysfunction that might derive from multiple oxidative actions of H_2O_2 within the cell.

Résumé

La sarcopénie est un syndrome gériatrique caractérisé par la perte progressive et âge-dépendante de la masse et force musculaire, accompagnée par des nombreux fardeaux personnels, économiques et sociétaux. Son incidence est estimée comme devant conduire vers une augmentation dans les années à venir, amenée par l'amélioration du système de santé et des conditions de vie.

Bien que le contexte étiologique de ce syndrome soit vastement hétérogène, des études récentes ont mis en évidence le rôle prépondérant de la mitochondrie et du dysfonctionnement mitochondrial dans son apparition. Le muscle squelettique, étant un tissu métaboliquement très actif, est particulièrement vulnérable aux dérèglements de la mitochondrie. Des altérations, même très légères, de la fonction mitochondriale peuvent se manifester par des signes cliniques importants.

Cette étude a été menée dans le cadre d'un projet R&D collaboratif financé par la Région de Wallonie, appelé MitoSir, qui rassemble plusieurs partenaires de recherche— notamment le laboratoire CORD (ULiege), RevaTis SA, GenFlow Bioscience et ULB— afin d'explorer le potentiel des cellules souches comme traitement pour la sarcopénie.

Dans cette étude, nous avons utilisé une lignée cellulaire de myoblastes humain immortalisés (LHCN-M2) et un traitement au peroxyde de d'hydrogène (H_2O_2) exogène dans le but de simuler un environnement oxydant potentiellement inducteur d'un dysfonctionnement mitochondrial, deux caractéristiques de la sarcopénie.

Nos résultats en utilisant de la Respirométrie à Haute Résolution (HRR) ont montré que les traitements à l' H_2O_2 exogène augmente la respiration leak de manière dose et temps-dépendante. La ETSmax a démontré une tendance à la diminution. Enfin, les résultats obtenus par le dosage CellTiter-Glo, utilisés pour quantifier le contenu cellulaire en ATP, appuient nos observations en montrant un écrasement des niveaux d'ATP de manière dose-dépendante suivant les traitements au H_2O_2 sans pour autant induire une mortalité cellulaire.
De manière globale, nos résultats pointent vers une dysfonction mitochondriale qui peut provenir de plusieurs actions oxydatives du H_2O_2 au sein de la cellule.

Introduction

(Note to reader: all images that do not contain any reference are personal and were done using BioRender).

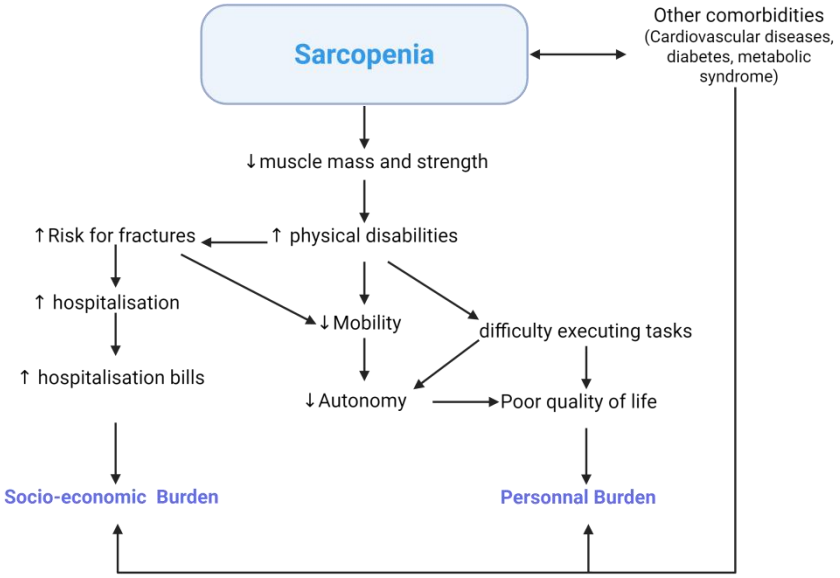

Image 1: Burdens of sarcopenia

.

Project context: brief presentation of the MitoSir project

MitoSir is a collaborative R&D project funded by the Wallonia-Federation, bringing together ULiege (CORD), ULB, Revatis SA Corp. and Genflow Bioscience. The project aims to explore the therapeutic potential of stem cells in the context of sarcopenia. Sarcopenia is a geriatic syndrome characterized by the progressive age-related loss of muscle mass and function (Park SS *et al,* 2017). This condition carries multiple personal, societal and economic burdens (Image1) and it is thought to impact an ever increasing number of people in developed countries (Kurnat-Thoma EL *et al*, 2022). This syndrome is also associated with other chronic comorbidities, such as cardiovascular disease, diabetes and metabolic syndrome (Damluji AA *et al*, 2023; Lena A *et al*, 2020)

While etiologies of sarcopenia remain heterogenous, studies have strongly associated it with inflammaging[1] (Liang Z *et al*, 2022; Wang T, 2022), oxidative stress (Tonkonogi M *et al*, 2003) and mitochodrial dysfunction (Frédéric N. Daussin *et al*, 2021; Marzetti E *et al*, 2013).

There are currently numerous drugs that are being used to target mitochondria, particularly in the context of cancer therapy. However, drug specificity, mitochondrial delivery, balance between therapeutic dosage and toxicity and variability among patients (Wang Q *et al*, 2024) represent major difficulties for the development of a treatment that targets mitochondria.

The idea behind MitoSir project is to develop a stem cell based therapy that could bypass all of these challenges in order to mitigate a mitochondrial dysfunction.

The goal of this master degree thesis is to develop a human *in vitro* model that simulates a mitochondrial dysfunction— one hallmark of sarcopenia— on which the different therapeutic approaches developed by the other partners could be tested on (Image 2).

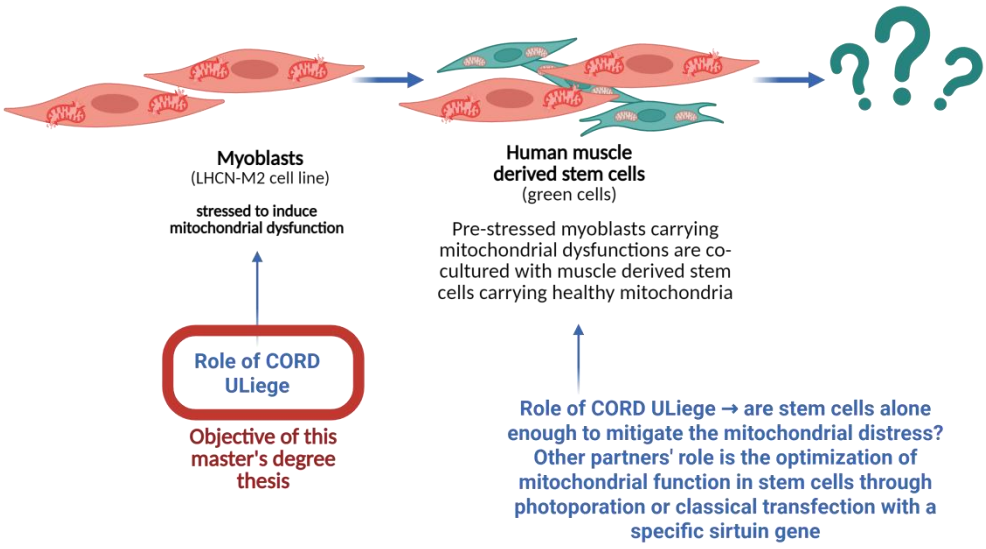

Image 2: Brief presentation of the MitoSir's project

[1] **Chronic inflammation that increases with the age; progressive inflammation linked to aging**

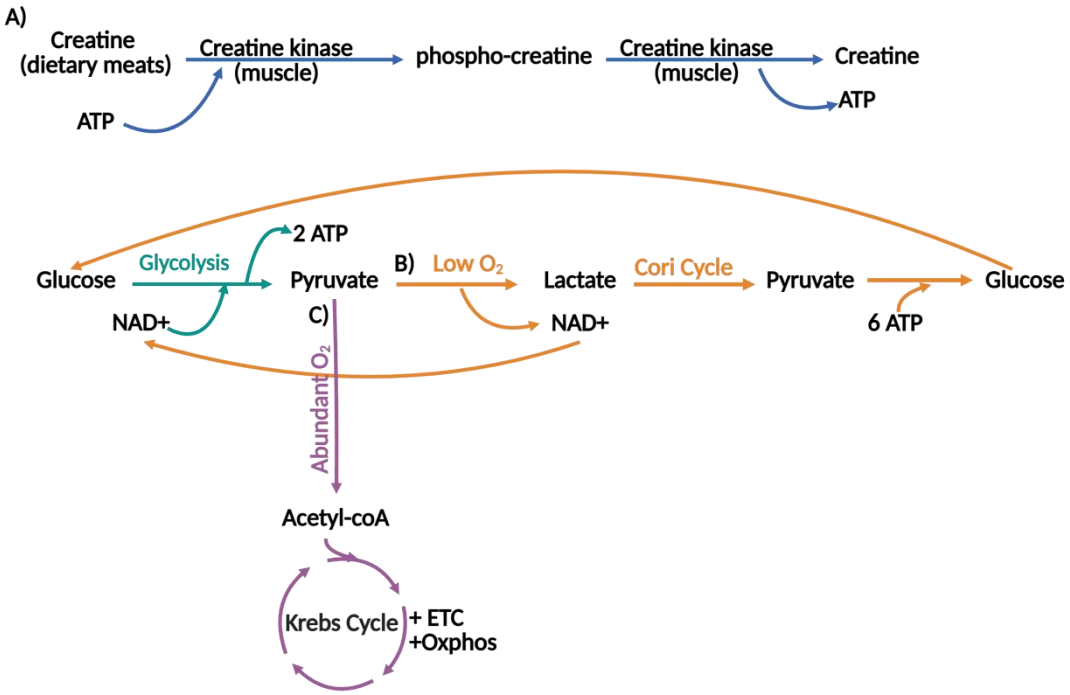

Image 3: Systems for ATP generation in skeletal muscle

A) Anaerobic alactic system: this is the fastest and simplest pathway for ATP production in muscle. It relies on stored phospho-creatine (PC) to produce ATP through the activity of creatine-kinase. Since this enzyme is mostly present in muscle tissue, it is used as a biomarker for muscle distress. For each PC there is only one ATP produced. However, phospho-creatine stores are limited and quickly depleted during longer efforts, making it incapable of meeting the required ATP demands.

B) Anaerobic lactic system: This system starts with glycolysis, where glucose is broken down into pyruvate, yielding a net of 2 ATP molecules per glucose. In the absence of oxygen, pyruvate is converted into lactate, which can be transported to the liver and recycled back to glucose via the Cori cycle (gluconeogenesis). This process requires 6 ATP molecules to regenerate glucose, which can reenter glycolysis to produce 2 ATP. While this system allows for ATP production during hypoxic conditions, by shifting the energy burden to the liver, it generates an energy imbalance that is highly inefficient and cannot be sustained long-term.

C) Aerobic system: Also initiated by glycolysis, this system operates when oxygen availability is not an issue. Pyruvate is transported into the mitochondria where it is converted into acetyl-coA, the first substrate of the Krebs cycle. This system, albeit more complex, enables the production of large amounts of ATP through oxidative phosphorylation.

Skeletal muscle tissue

Muscle tissue is essential for producing force and to allow movement of the organ or structures to which it is related. There are 3 types of muscle tissue in the human body— skeletal, cardiac and smooth— and even though they share common features (excitable, contractile, extensible and elastic), each one of these tissues is highly specialized and have their own specific characteristics that allow them to fulfill different functions (Biologie Anatomie Physiologie, Nicole Menche, 9th edition, ISBN: 978-2-294-77396-9).

Skeletal muscle sustains important physiological functions such as voluntary movement, postural stability, balance and even breathing.

Skeletal muscle fibers are long (5cm) post-mitotic cells, multinucleated, originated from the fusion of multiple precursor cells called myoblasts. Their cellular membrane is called sarcolemma and surrounds the sarcoplasm. Because these cells have a high energy demand, their sarcoplasm contains glycogen (glucose-based macromolecule) and myoglobin (carrier of O_2).

Satellite cells are adult stem cells found between the basal membrane and the sarcolemma. They can proliferate and differentiate into muscle fibers and are responsible for muscle growth and regeneration during lesion.

The sarcolemma is extremely important for the functioning of skeletal muscle as it forms expansions called T-tubules (Image 4), which concentrate voltage-gated calcium channels and bring them to close proximity with the sarcoplasmic reticulum, which stocks the majority of the intracellular calcium.

Skeletal muscle fibers contain contractile elements (actin, myosin and titin proteins) organized in sarcomeres (contractile units) which depend on ATP to function. Despite the high energy requirements, skeletal muscle stores only enough ATP to ensure efforts of merely few seconds (Picca A *et al*, 2021). Therefore, it must rapidly adapt to support more sustained efforts by generating additional ATP.

There are 3 main pathways which allow the renewal of ATP within muscle cells (Image 3) (Baker JS *et al*, 2010):

Skeletal muscle contains creatine-kinases which utilize stored phospho-creatine to produce ATP (Image 3 A). This enzyme is mostly present in the muscle tissue and is often used as a biomarker for muscle distress. While this system is relatively simple, it only produces one ATP molecule per phospho-creatine and does not meet the energy requirements under more demanding efforts.

The anaerobic lactic system (Image 3 B) is the second process through which muscle can produce ATP. This system begins with glycolysis, which allows the production of 2 ATP molecules through the breakdown of glucose into pyruvate. In hypoxic conditions, pyruvate is converted into lactate, which can

be transported into the liver and enter the Cori cycle. This cycle allows to regenerate glucose from lactate (gluconeogenesis) but it requires 6 ATP molecules in order to do so. Although this system allows ATP production under hypoxic conditions by shifting the energy deficiency from the stressed active muscle to the liver (Visavadiya NP *et al*, 2021), it creates an energy imbalance that cannot be favorable to long-term efforts (Monireh Dashty, 2013).

Finally, in the aerobic energy system (Image 3 C), when oxygen is readily available, pyruvate enters the mitochondria and is converted into acetyl-coA. This initiates the most complex—but also the most efficient—pathway for ATP production: oxidative phosphorylation (OXPHOS). Through his process, the muscle can generate a large amount of ATP (roughly 30 ATP molecules per glucose), making it essential to maintain prolonged physical activity. This highlights the critical role of mitochondria in supporting muscle function mostly through energy production.

For this reason, muscle tissue is packed with mitochondria which can adapt in number and size according to the frequency and duration of the efforts.

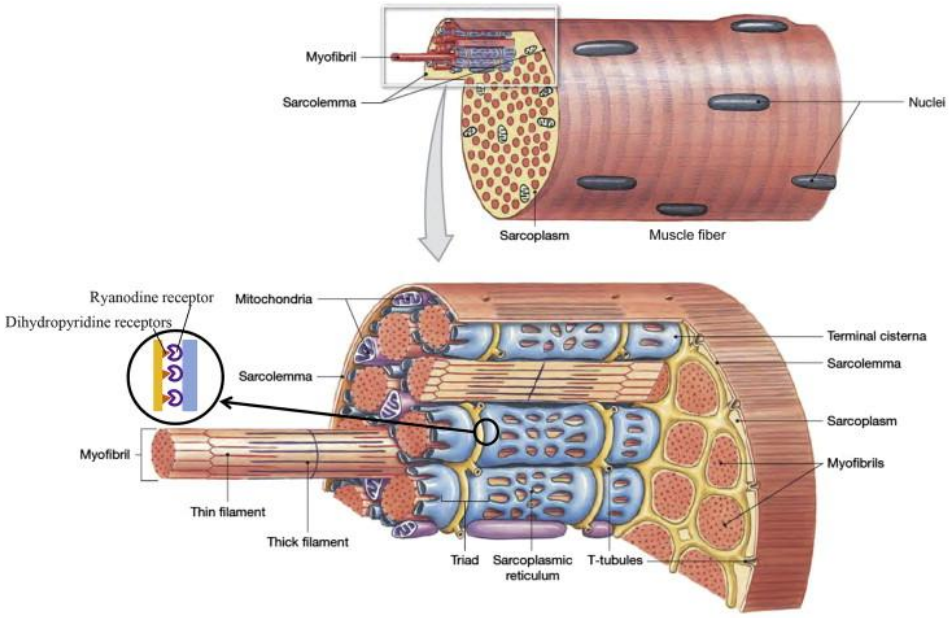

Image 4: Skeletal Muscle Structure- Importance of T-Tubules

(S.K. Gollapudi et al, 2014)

Mitochondria

1. Structure and function

Mitochondria are intracellular organelles present in most eukaryotic cells. Commonly referred to as the “powerhouse of the cell”, they play a vital role in energy production (ATP), which makes these organelles especially important for the sustaining of homeostasis and life. In fact, they are the very reason why we need the oxygen we breath and a heart to distribute it.

Despite their well-known role in ATP production, mitochondria are also key regulators of several other cellular processes, including calcium and protein homeostasis and programmed cell death (apoptosis)(Image 5). Calcium alone regulates important cellular processes such as fusion of neurotransmitter vesicles in the neurons or vesicles containing insulin in the pancreas, contraction and relaxation mechanism in the muscles, activates numerous transcription factors and cellular enzymes. Given the central role of mitochondria for cellular homeostasis, there are systems for the mitochondrial quality control. These include fusion, fission, mitophagy and mitochondrial protease systems (Emanuele Marzetti *et al*, 2024).

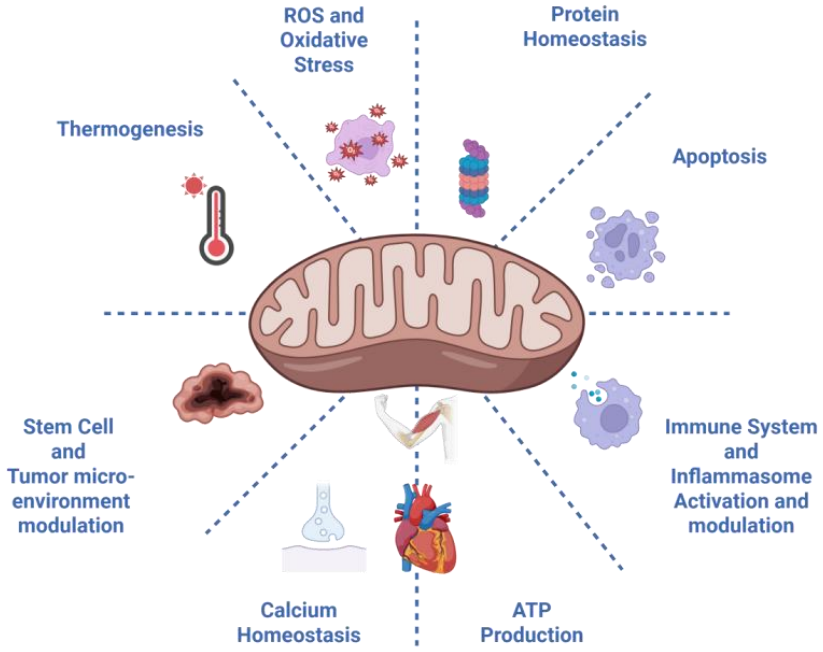

Image 5: Non exhaustive list of mitochondrial functions within cells

Some distinctive features of mitochondria are the presence of their own DNA (mtDNA), two bi-layered lipid membranes and 70s ribosomes— three characteristics that support the theory of an endosymbiotic origin between a primitive eukaryotic cell and an ancestral prokaryote.

Although the mitochondrial genome encodes for 13 polypeptides, 22 tRNAs and 2 rRNAs (Anderson S *et al*, 1981) involved exclusively in mitochondrial metabolism, approximately 99% of its proteome is

composed of nuclear-encoded proteins synthesized by cytosolic ribosomes. This highlights the semi-autonomous nature of these organelles (Shen X *et al*, 2022) and the complexity of its functionality. The mitochondrial inner membrane (MIM) has a particularly interesting composition (Colina-Tenorio L *et al*, 2020) . It possesses a unique phospholipid— cardiolipin— and is highly impermeable to protons. While this impermeability is crucial for maintaining the proton gradient necessary for ATP production —achieved through the coupling of an electron transport chain (ETC) with an oxidative phosphorylation (OXPHOS) (Image 6)— cardiolipin is important to the stabilization of mitochondrial complexes, for the formation of the mitochondrial cristae and regulation of apoptosis. Because it contains unsaturated fatty acids, it its highly vulnerable to oxidation, which can increase membrane permeability (Panov AV *et al*, 2020).

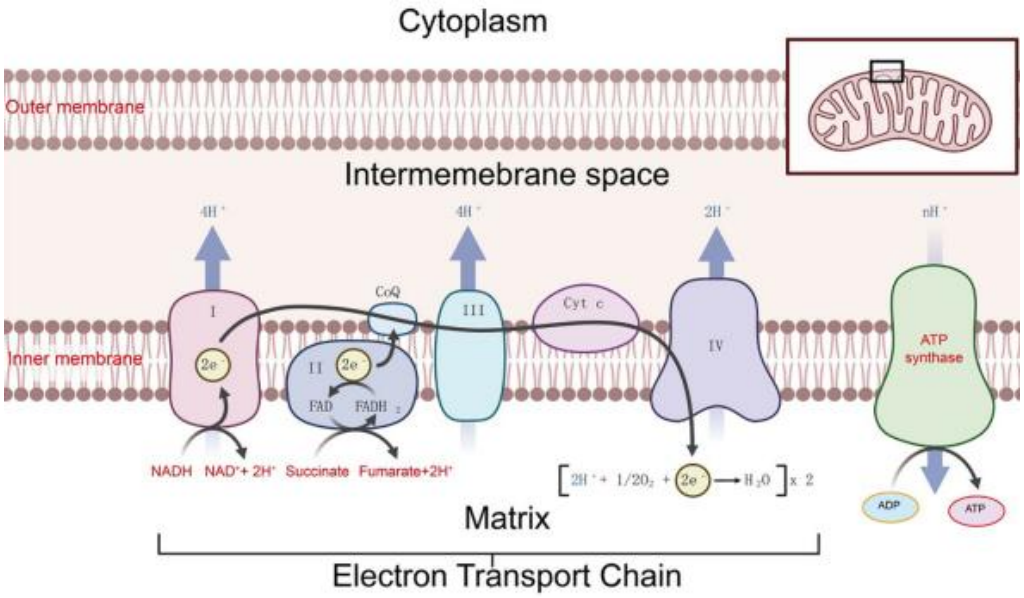

Image 6: Electron Transport Chain (ETC) and OXPHOS

Complex I: NADH dehydrogenase.

Complex II: succinate dehydrogenase

Complex III: Ubiquinol-cytochrome c reductase

Complex IV: cytochrome c oxidase

Complex V: ATP synthase

(Wang Q *et al*, 2024, DOI: 10.3389/fimmu.2024.1520072)

2. Krebs cycle and electron transport chain (ETC)

Mitochondrial energy production relies heavily on the oxidation of carbohydrates, fats and proteins into Acetyl-CoA to produce energy in the form of ATP (Image 7 A).

Glycolysis is the most frequent process through which mitochondria obtain acetyl-coA. During glycolysis, cells break down glucose contained in carbohydrates into pyruvate, which accumulates in the mitochondrial matrix and is converted into acetyl-coA by a pyruvate dehydrogenase.

Acetyl-coA is the first substrate of the Krebs cycle (Image 7 B) (also known as citric acid cycle or TCA), a series of enzymatic reactions that extract electrons to reduce cofactors NAD+ and FAD+ into NADH and $FADH_2$. The energy stored in sugars is transformed and temporarily carried by NADH and $FADH_2$ whose role is to transfer this energy to the electron transport chain (ETC) through complexes I and II located on the inner membrane of mitochondria (Arnold PK *et al*, 2023).

The electron transport chain is a redox chain consisting of four protein complexes coupled with a fifth complex (Image 7 C) responsible for ATP production (Cogliati S *et al*, 2021).

Complexes I and II process NADH and $FADH_2$ —produced in the Krebs cycle and glycolysis— removing electrons and extracting their energy to pump protons against their gradient through complexes I, III and IV. As electrons pass through the ETC complexes, their free energy decreases.

In complex IV, molecular oxygen (O_2) is the final electron acceptor (has the biggest redox potential). Complex IV combines the extracted electrons with protons and molecular oxygen to form water.

Complex V, or ATP synthase, utilizes the chemiosmotic proton gradient created by the ETC complexes to produce ATP. For every three protons that flow through complex V, approximately one ATP is produced. Pinpointing the exact number of ATP produced will always be an approximation because, even though the mitochondrial inner membrane has a relatively low permeability, some protons still leak across the membrane, reducing the efficiency of the coupling between ETC activity and ATP production (Divakaruni AS *et al*, 2011).

To maximize the coupling between ETC and ATP synthesis, to decrease the risks of electron slip or proton leakage, complexes I to V are associated with one another to form a functional assembly in the mitochondrial cristae, called respirasome. Besides cardiolipin, the formation of these membranous folds is also possible thanks to complex V which, in addition to its role in ATP production, also contributes to the ultra-structure of the inner mitochondrial membrane (Strauss M *et al*, 2008). The cristae increase the surface area for the formation of more OXPHOS complexes and reduce the distance of diffusion of the different substrates produced in the Krebs Cycle, thereby enhancing the efficiency of ATP synthesis. These folds are also important to allow the dual activity of complex II, which participates both in the Krebs cycle and in the ETC (reason why it is the only complex that is not a proton pump).

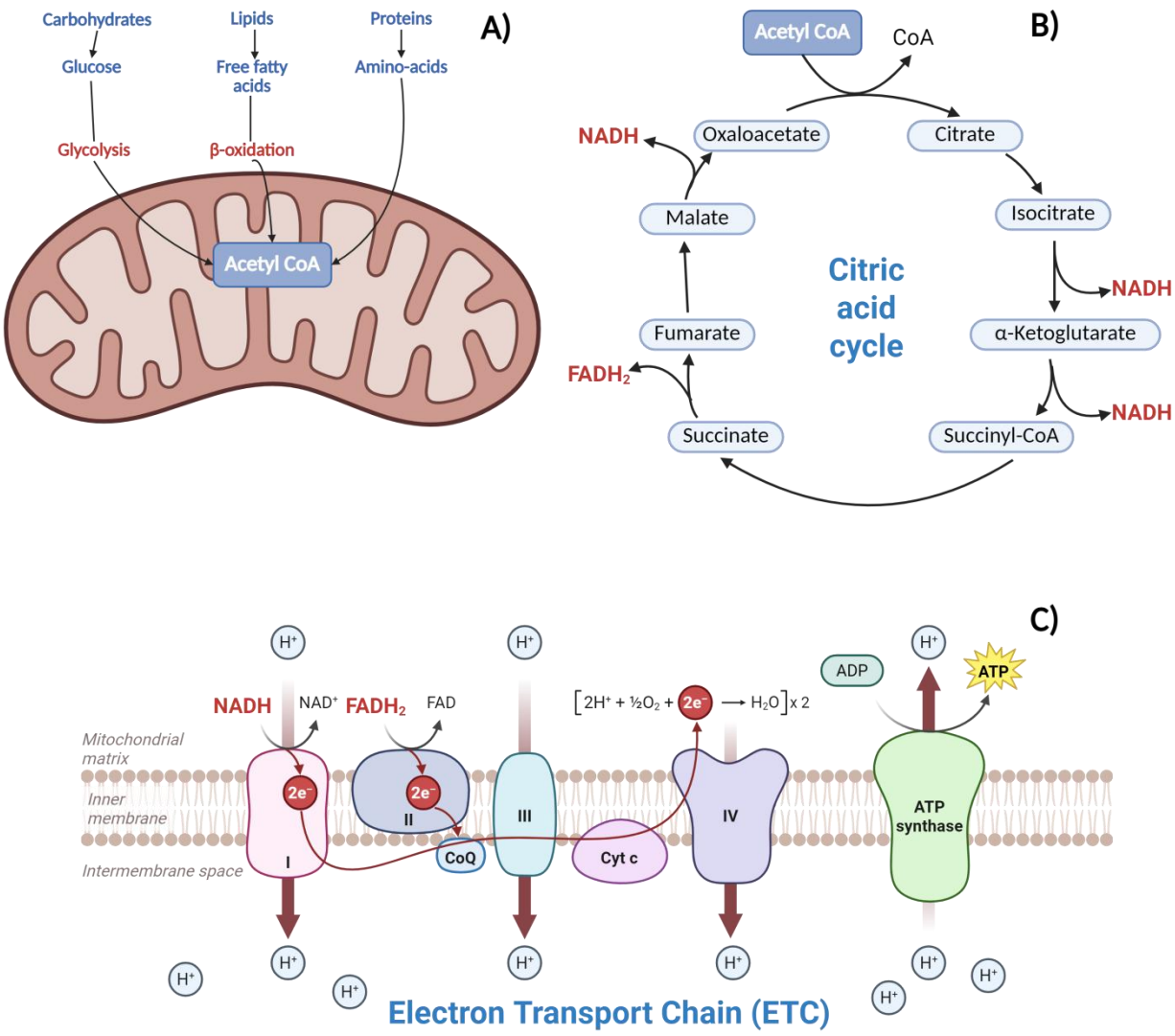

Image 7: Summary of mitochondrial metabolism

A) Acetyl-coA can be produced through the breakdown of macro-molecules and utilized by mitochondria to generate ATP

B) Acetyl-coA is the first substrate of the Krebs cycle which allows the production of co-factors NADH and $FADH_2$.

C) The electron transport chain (ETC) uses electrons from co-factors NADH and FADH2 to allow ATP production

3. Reactive Species (RS) and Oxidative Stress (OS)

Aerobic cellular respiration is inherently linked to oxidative stress. Cells with high metabolic needs—such as cancer cells and skeletal muscle— tend to generate increased levels of reactive oxygen species (ROS), primarily within mitochondria.

During normal cellular metabolism, some of the oxygen consumed is not reduced to water. Indeed, electrons can leave the electron transport chain and can be prematurely combined to molecular oxygen, forming the superoxide anion (O_2^-) (Gisela Storz *et al*, 1999) which can be converted into other ROS (H_2O_2, HOCl) as well as into reactive nitrogen species (RNS) (peroxynitrite $ONOO^-$, nitric oxide NO•, nitrogen dioxide NO_2•). Therefore, ROS are sometimes considered a normal byproduct of the electron transport chain.

Reactive oxygen species have a dual role within cellular metabolism.

At lower concentrations (usually 1-100nM) they mainly regulate cell signaling and promote cell proliferation (Liu S *et al*, 2022)—often referred to as oxidative eustress. H_2O_2 is especially important for redox signaling, acting as a second messenger, along with H_2S (hydrogen sulfide) and NO (nitric oxide) (Di Marzo *N et al*, 2018). However, at higher concentrations (usually above 100nM) their toxicity becomes more prominent, provoking macromolecular damage. Indeed, their highly reactive chemical structure makes them prone to bind to larger molecules such as proteins, nucleic acids and lipids, altering their structure and function (Chaudhary MR *et al*, 2023). In this case we refer to as oxidative distress (Chalifoux O *et al*, 2023).

Oxidative stress can be extremely harmful to cells, to such extent that it is used as a natural defense mechanism to kill bacteria *in vivo* (Gisela Storz *et al*, 1999). This discovery made it possible to use H_2O_2 in the medical field as a topic antiseptic for wound cleaning or in labs as a way to sterilize surfaces and materials (Ayub A *et al*, 2024). In animals and humans neutrophils engulf pathogens and metabolize H_2O_2 into a more dangerous ROS, HOCl, through enzymatic activity of myeloperoxidase (MPO). HOCl is a potent antimicrobial oxidant.

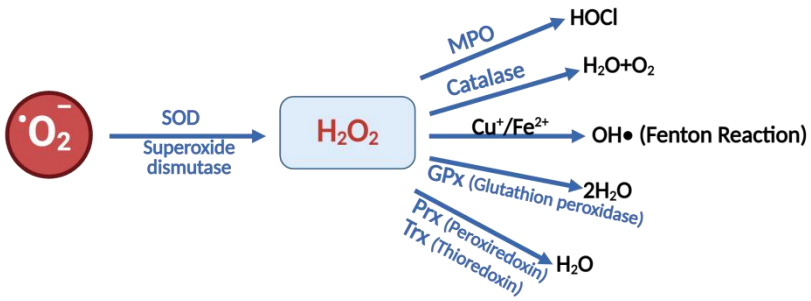

Image 8: Enzymatic antioxidant systems for H_2O_2 detoxification

Endogenous hydrogen peroxide (H_2O_2) can be directly generated by oxidoreductases and dehydrogenases such as α-ketoglutarate and pyruvate dehydrogenase, two enzymes of the Krebs Cycle (Chalifoux O *et al*, 2023). H_2O_2 can also be indirectly obtained through dismutation of the superoxide anion ($O_2^{\cdot-}$) by an enzyme called superoxide dismutase (SOD), present in mitochondria (matrix Cu/Zn-SOD1 and Mn-SOD2 in the intermembrane space), cytoplasm (Cu/Zn-SOD1) and even extracellular space (Zu/Zn-SOD3). Dismutation of the superoxide anion is just one of several mechanisms that cells employ to scavenge ROS and prevent oxidative stress, thereby protecting macromolecules from oxidative damage.

These antioxidant defense systems are diverse and include enzymatic, non-enzymatic and repair/removal mechanisms.

For instance, H_2O_2 can be neutralized using several peroxidases (Image 8), including glutathione peroxidase (GPx), thioredoxin peroxidase (Trx) and catalase. Alternatively, H_2O_2 may react with complexed ferrous iron (Fe^{2+}) in the Fenton Reaction, which leads to the production of $OH^{\bullet}$, another unstable, highly reactive ROS.

Therefore, maintaining a balance between ROS and antioxidant mechanisms is crucial for cellular homeostasis and overall cellular fitness. When this equilibrium is disrupted, either through excessive ROS production or insufficient ROS scavenging, oxidative stress occurs. Mitochondrial proteins, lipids and DNA are especially susceptible to oxidative damage due to their proximity to ROS formation sites. Moreover, mtDNA is not protected by histones and possesses limited repair capacities.These vulnerabilities make mtDNA especially prone to oxidative lesions, which can trigger a self-perpetuating cycle of mitochondrial mutations, ROS formation and impaired bioenergetics ultimately paving the way to cell damage and death.

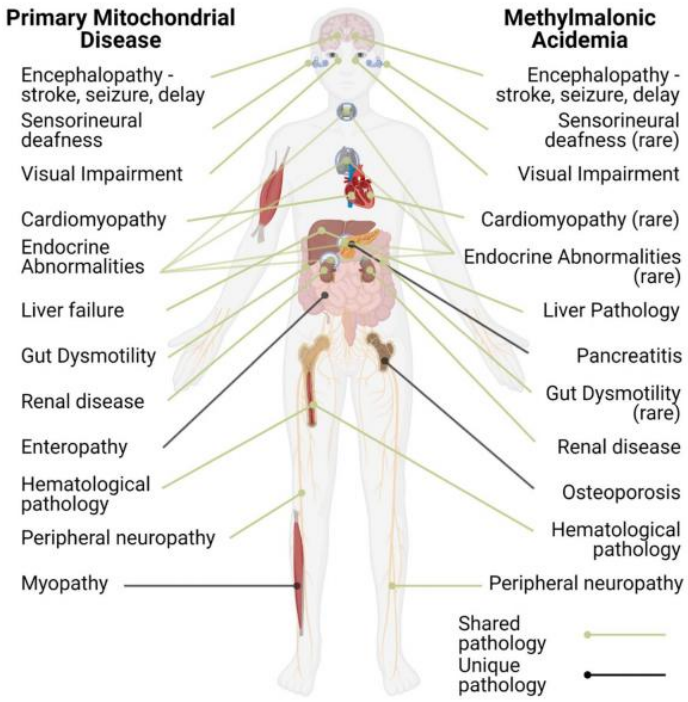

Image 9: Comparison of clinical manifestations of a primary mitochondrial dysfunction and a mitochondrial dysfunction secondary to mutations that indirectly affect mitochondrial function

(Luciani A *et al*, 2021)

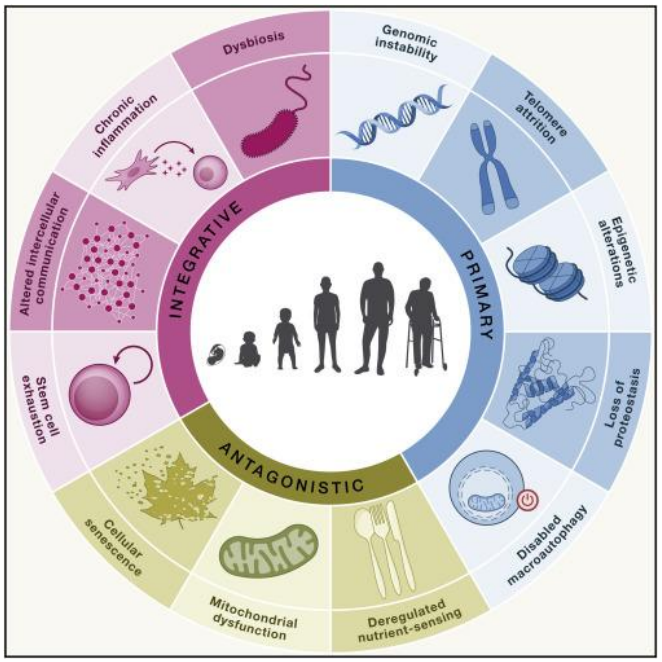

Image 10: Hallmarks of aging **(López-Otín C *et al*, 2023)**

4. Mitochondrial dysfunction in aging and disease

Aging is intricately linked to mitochondrial dysfunction (Alexander V Panov *et al*, 2020), although it remains largely unclear whether this dysfunction is a cause or a consequence of aging and diseases (Luciani A *et al*, 2021**)** (Figure 9). Primary mitochondrial dysfunctions, caused by mutations that directly impair mitochondrial proteins lead to multisystemic vulnerabilities and a wide range of clinical manifestations. Many of these symptoms are nonspecific and overlap with those found in diseases that induce secondary mitochondrial dysfunctions, complicating both diagnosis and therapeutic strategies.

A consistent finding across studies is the strong correlation between aging, increased oxidative damage and chronic low-grade inflammation (Marzetti E *et al*, 2013). Human studies have shown that aging is associated with a decline in OXPHOS capacity, reduced ATP production and upregulation of antioxidant proteins (Holloway GP *et al,* 2018; Porter C *et al,* 2015; Short KR *et al*, 2005; Greco M *et al*, 2003). Age-related comorbidities typically affect systems with high energy demands, such as nervous, cardiovascular, musculoskeletal and immune systems, all of which share a common pathological ground: mitochondrial dysfunction. Indeed, mitochondrial impairments appear to be central to the pathogenesis of numerous age-related diseases, including sarcopenia (Ferri E *et al*, 2020; Marzetti E *et al*, 2013), heart failure, diabetes, hearing loss, rheumatoid arthritis, cancer, neurodegenerative disorders such as Parkinson's, Alzheimer's diseases (Kamarulzaman NT *et al*, 2025) and even age-related hearing-loss (Ege T *et al*, 2024). In the brain, mitochondrial structure and mitochondrial quality control systems (MQC)[2] are often disrupted and the release of mitochondrial components —such as mtDNA, cytochrome c, cardiolipin— installs a pro-inflammatory environment that activates microglia, which could be the starting point of many neurodegenerative diseases or even brain cancers (Shen X *et al*, 2022).

To put it in more general terms, any mitochondrial dysfunction— whether primary or secondary—leads to disturbances of key aspects of cellular physiology (e.g. imbalances in calcium homeostasis, reduced ATP content and energy reserves, increased ROS levels, increased damage to macromolecules,etc). Finally, most—if not all— ATP-dependent processes such as autophagy, apoptosis, mitophagy, translation, transcription, protein degradation by the proteasome, are also disrupted.

Overall, the loss of mitochondrial integrity is widely attributed to dysfunctions in mitochondrial quality control mechanisms (MQC), hormonal imbalance and mutations in both mitochondrial (mtDNA) and nuclear (nDNA) DNA.

While mitochondrial dysfunction is currently recognized as one more hallmark of aging, it also plays a central role in driving many of the other hallmarks. The central role of mitochondria in both physiology and pathogenesis makes them a compelling target to study aging, age-related diseases and other disorders associated with mitochondrial dysfunction.

---

[2] **MQC processes involve proteostasis, mitochondrial biogenesis, mitophagy, fission, fusion**

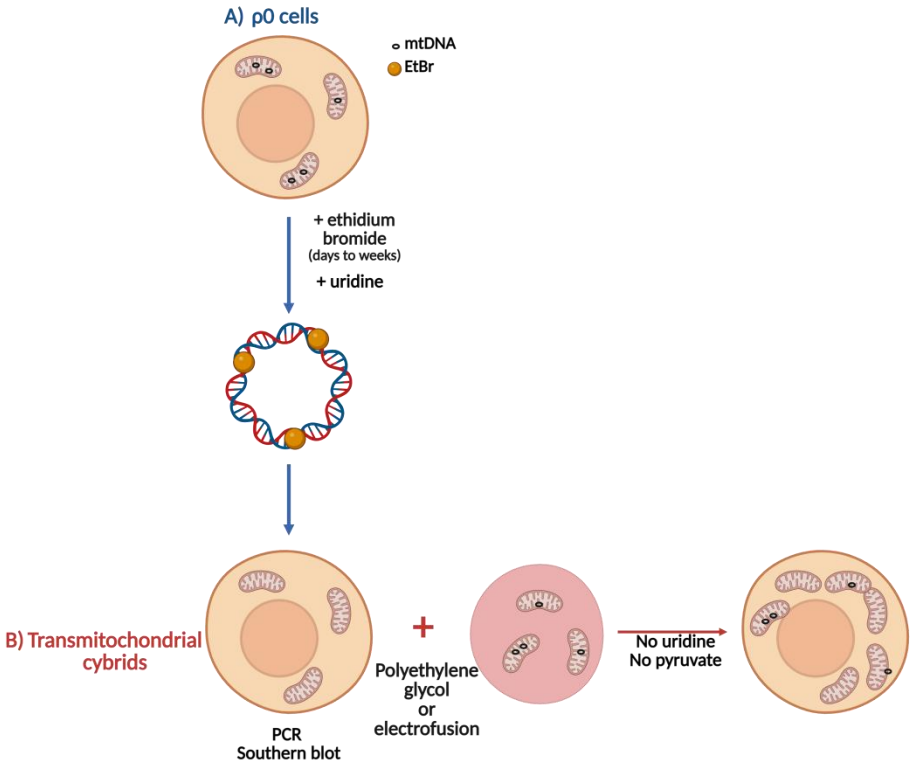

Image 11: Summary of the process through which ρ0 cells and transmitochondrial cybrids can be obtained.

A) To generate ρ0 cells, cells are cultured for weeks in the presence of low dosages of ethidium bromide (EtBr). EtBr possesses positive charges that bind to the negative charges of DNA. Because mtDNA is not protected by proteins, intercalating agents such as EtBr at low doses can selectively bind to mitochondrial DNA. This interaction inhibits the activity of the polymerase γ and thus replication of mitochondrial DNA. Cells are let in culture for a couple of weeks, provided with supplements such as uridine, to allow viability. After several cellular divisions, mitochondria should be depleted of DNA. PCR or southern blottings can be done in order to assess this.

Fernández-Moreno M *et al*, 2016, Generating Rho-0 cells using mesenchymal stem cells lines, DOI: 10.1371/journal.pone.0164199

B) Transmitochondrial cybrids are formed from ρ0 cells, which conserve their nuclear DNA but contain mtDNA-depleted mitochondria.

ρ0 cells are fusionned with cells that are anucleated and provide a specific mtDNA context.

Polyethylene glycol (PEG) or electrofusion is used to fusion the cells.

Fusion products are cultured without pyruvate nor uridine, in order to select only cells that contain functional mitochondria.

Pye D *et al*, 2006, Production of transmitochondrial cybrids containing naturally occuring pathogenic mtDNA variants, DOI: 10.1093/nar/gkl516

5. Types of *in vitro* models for mitochondrial function

To investigate the impact of mitochondria on cellular metabolism, several experimental models have been used. ρ0 cells (Image 11 A) are depleted of mtDN and are commonly used to evaluate the contribution of mtDNA to cellular mechanisms (Fernández-Moreno M *et al*, 2016). Additionally, transmitochondrial cybrids (Image 11B)— cells with similar nDNA but different mtDNA— allow researchers to study the impact of different mtDNA backgrounds on cellular function (Pye D *et al*, 2006). More targeted approaches involve gene therapy techniques or RNA interference to induce mutations in the nuclear or mitochondrial genes. Another widely used strategy is the application of specific inhibitors that target mitochondrial complexes, effectively altering the coupling between ETC and oxidative phosphorylation thus mimicking a mitochondrial dysfunction.

Other models that disrupt mitochondrial function include serum starvation, hypoxia and TNF-α treatment, all of which interfere with mitochondrial activity.

Additionally, it is also possible to recreate an oxidative environment by inhibiting the antioxidant defense systems, tipping the redox balance towards ROS accumulation. The choice of strategy and molecular targets depends heavily on the etiological context of the disease that is being modeled.

In the case of sarcopenia, the exact pathophysiological mechanisms remain largely unclear and highly heterogenous. However, oxidative stress and mitochondrial dysfunction are widely accepted hallmarks of the syndrome and other age-related diseases (Image 10) (López-Otín C *et al*, 2023).

Therefore, in this project, we have chosen to use hydrogen peroxide (H_2O_2)— a central reactive oxygen species— as a tool to mimic an oxidative stress that could induce a mitochondrial dysfunction.

5.1. Exogenous H_2O_2 treatment as an *in vitro* model for mitochondrial dysfunctions

Usually, only small non-charged molecules can bypass biological membranes by simple diffusion. H_2O_2 is the most stable ROS and highly hydrophilic which means it should not normally pass the cell membranes. However, because it has a similar dipole moment to that of the water molecule, its transport across cytoplasmic membranes can be facilitated by aquaporins (Bienert GP *et al*, 2006; Bienert GP *et al*, 2007; Bienert GP *et al*, 2014).

Xin X *et al* (2022) used H_2O_2 as a means to investigate the effect of an oxidative stress on meningothelial cells of the optic nerve. In their article they demonstrated that H_2O_2 decreases cell viability, alters cell morphology and increases ROS levels.

In another study, exogenous H_2O_2 increased mitochondrial fragmentation and reduced mitochondrial membrane potential of myoblasts (Iqbal S *et al,* 2014).

Finally, lipid peroxidation can be formed through ROS exposition and affect membrane structure, integrity, flexibility and permeability (Gaschler MM *et al*, 2018; Catalá A *et al*, 2016).

Even though many studies have been led demonstrating the effect of exogenous H_2O_2 on different cell types including meningothelial cells (Xin X *et al*, 2022) and a rat myoblast cell line C2C12 (Siu PM *et al*, 2009), little to no research has been conducted using muscle human models, such as LHCN-M2 cell line. To our knowledge there is one study in which researchers applied an exogenous H_2O_2 stress on the LHCN-M2 cell line, demonstrating its effet on ROS production but not on mitochondrial respiration dynamics (Mancini A et al, 2022).

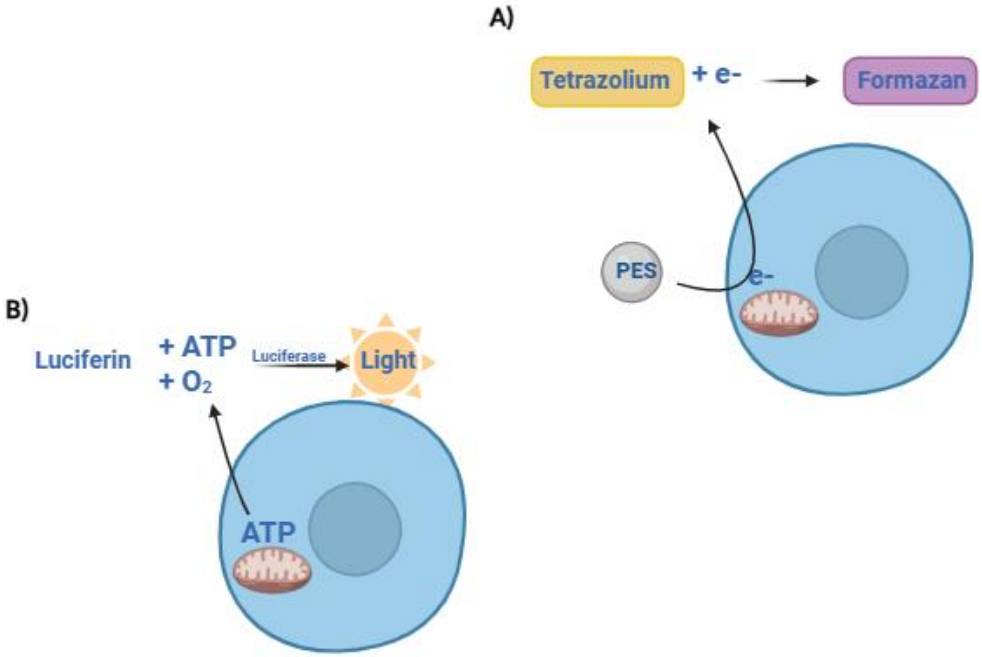

Image 12: Schematic representation of how MTS and CellTiter-Glo assays work

A) MTS assay is a fluorescence based assay that relies on the conversion of tetrazolium salts into formazan compound (λex/em:490nm/500-520nm) by mitochondrial NADH-dependent dehydrogenases.

B) CellTiter-Glo assay is a chemiluminescent assay that relies on the activity of luciferase to oxidize luciferin into oxyluciferin in the presence of ATP

Analysis for mitochondrial function

1. MTS and CellTiter-Glo assays

MTS is a variant of the tetrazolium compound that can be reduced and converted to formazan dye, which is soluble and its absorbance can be measured at 490-500nm (Image 12 A) by a spectrophotometer.

The MTS assay relies primarily on the activity of mitochondrial NADH-dependent enzymes (for example mitochondrial complex I) and to a lesser extent to other dehydrogenases, such as mitochondrial complex III. Thus, it can provide valuable information into how well the ETC is working.

NADH dehydrogenases extract elecetrons from NADH cofactors and act as electron donors. Since biological membranes are not permeable to tetrazolium compounds, the use of electron transporters is required (usually PES or PEM solutions provided in most MTS kits).

In living cells, dehydrogenases are active and MTS signal is high. In dead cells, dehydrogenases do not work and the MTS signal is low. For this reason, MTS assay is widely used as a viability measure. However, this should be taken lighly as the MTS assay is more accurately defined as a metabolic assay. Indeed, if a stress is applied to cells, they can decrease their metabolism and give decreased MTS readouts even though the cells are alive. For this reason, MTS assay should be coupled to complementary viability tests, such as trypan blue exclusion or sytox green.

CellTiter-Glo is a chemiluminescence-based assay used to quantify intracellular ATP content (Image 12 B). For this assay, cells need to be lysed to release the cytoplasmic content, such as mitochondrial ATP. The ATP is used by luciferase which, in presence of O_2, oxidizes luciferin to oxyluciferin, producing light. The amount of light produced is proportional to ATP content of cells. The emitted light can be detected using a luminometer. Similarly to MTS, CellTiter-Glo is also widely considered a viability test. Indeed, ATP is essential for the maintaining of life and it is not present in dead cells. However, just as for the MTS assay, CellTiter-Glo can more broadly reflect cellular metabolism and should also be coupled to complementary viability assays.

Both MTS and CellTiter-Glo assays can indirectly provide insights into mitochondrial function and overall cellular metabolism or viability. During mitochondrial dysfunction, ATP production may decline, leading to a reduction in CellTiter-Glo signals. Similarly, impairments in the electron transport chain (ETC) can disrupt electron flow, resulting in decreased MTS assay readouts. In non-viable cells, mitochondria undergo mitophagy, which could be reflected by diminished signals in both assays.

However, for more robust and precise analysis of mitochondrial function, high-resolution respirometry can also be used.

2. High-Resolution Respirometry (HRR)

2.1. Principle

High Resolution Respirometry (HRR) measures the O_2 concentration in a closed system. OROBOROS oxygraphs contain two independent glass chambers each connected to a polarographic oxygen sensor (POS) composed of platinum cathode and an Ag/AgCl anode in a KCl solution and a O_2 permeable membrane. Dissolved O_2 is reduced to water by electrons at the cathode.

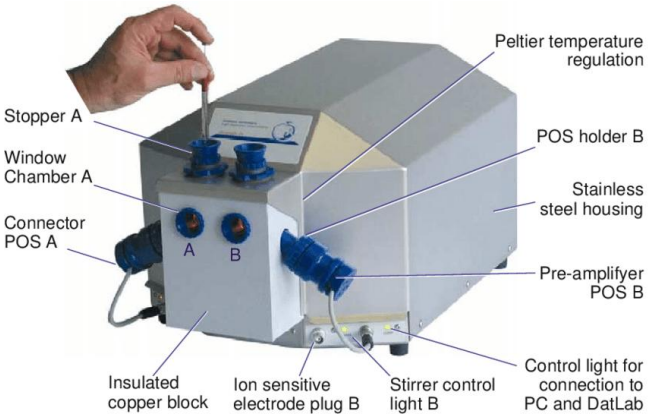

Image 13: Description of O2K oroboros oxygraph **(Hütter E *et al*, 2006, DOI: 10.1016/j.exger.2005.09.011)**

Each chamber has a capacity of 2ml and can be closed by a stopper which contains a rubber ring to allow samples to be completely air-sealed or to be relatively permeable to air when the stopper is not fully tightened. The stopper also contains a small capillary entry from which substrates, inhibitors, uncouplers, light guides or other sensors can be added.

2.2. Protocol used to assess mitochondrial function in living cells (SUIT-003)

Oroboros proposes various protocols to assess mitochondrial respiration.

In this study, we used the SUIT-003 protocol for living cells (Pesta D *et al*, 2012).

The principle consists on the inhibition of a single complex at a time in a specific order to see how it affects oxygen concentration in the chambers, giving an indirect measure of mitochondrial respiration.

The chambers need to be calibrated with 2ml of air-saturated medium (chambers not closed by the stopper) to allow background corrections for instrument function before each analysis.

After calibration with culture medium, cell suspension samples can be added to the chambers which will then be closed with the stoppers.

We can follow the evolution of two slopes throughout time: the O_2 concentration slope (blue line) and the O_2 flux (red line) which translates the oxygen consumption rate (OCR) by cells (cellular respiration)(Image 15).

Data can also be expressed as flux control ratios (FCR) to evaluate the functional equilibrium between the different respiratory states (Routine, Leak, oxphos etc).

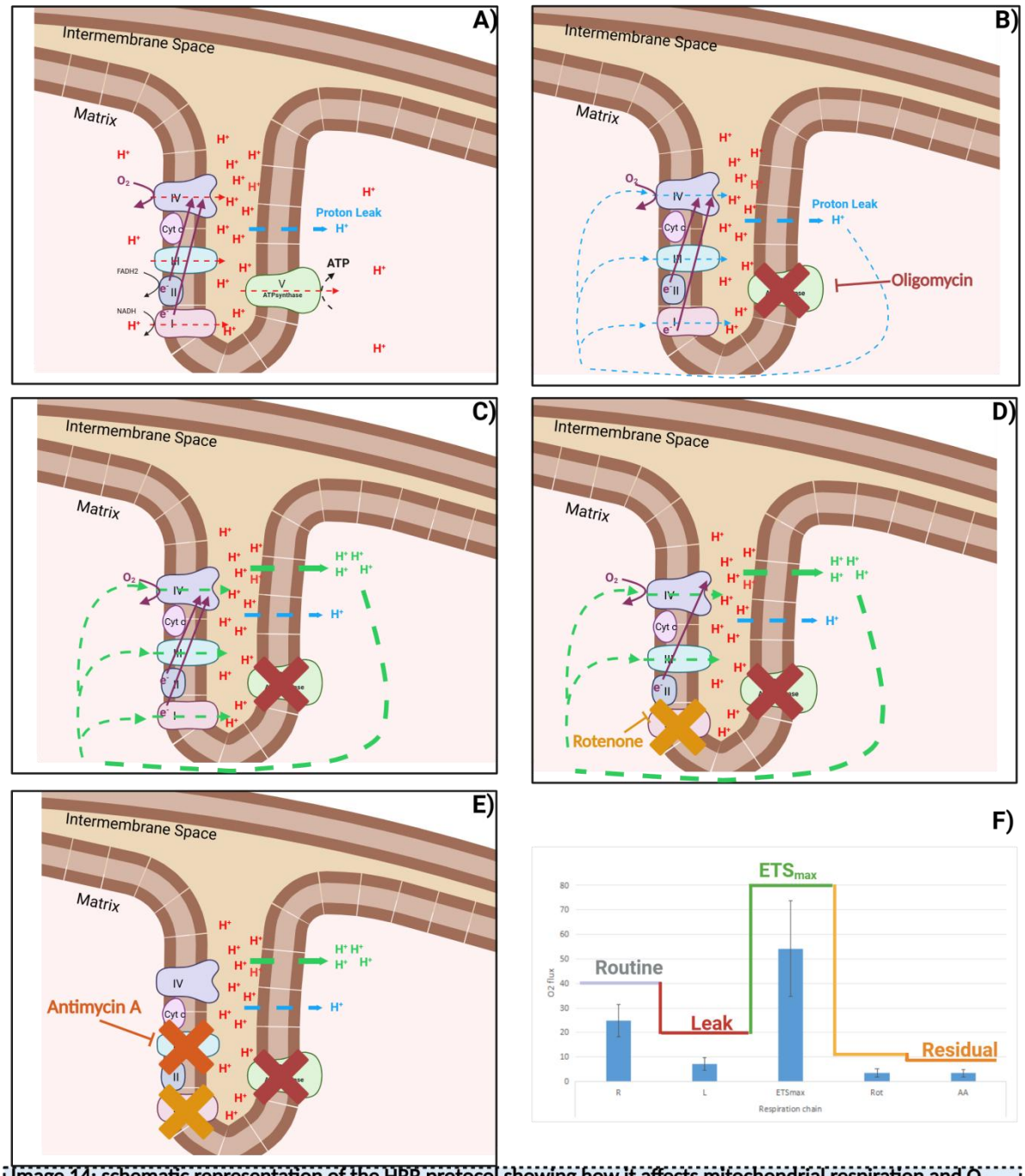

Image 14: schematic representation of the HRR protocol showing how it affects mitochondrial respiration and O_2 flux values

A)Routine respiration (basal respiration). ATP synthase uses a protonmotive gradient to produce ATP. This gradient is created by complexes I, III, IV and the permeability of the inner mitochondrial membrane. Basal proton leakage dissipates the gradient.

B) Leak respiration (after inhibition of ATP synthase with oligomycin). Only the leaked protons sustain the activity of complexes I, III, IV and O_2 consumption.

C) ETS_{max} respiration after titration with an uncoupling agent (FCCP). FCCP passes easily through the mitochondrial inner membrane transporting protons. It allows the complexes I, III and IV to work at full capacity without limitations due to membrane impermeability nor ATP synthase activity.

D) complex II respiration (after inhibition of complex I by rotenone). The mitochondrial chain can still work but at a less sustained level. Electrons can still enter the ETC through complex II and be translocated to Complex IV where it is combined to O_2 to form water.

E)Residual respiration after inhibition of complex III with antimycin a. Since complex III is the convergence site of electrons, its inhibition prevents the ETC to work. There is not O_2 consumption by mitochondria. Any O_2 consumption detected at this point is not due to mitochondrial activity.

F) Graphic displaying O_2 flux after addition of each substrate.

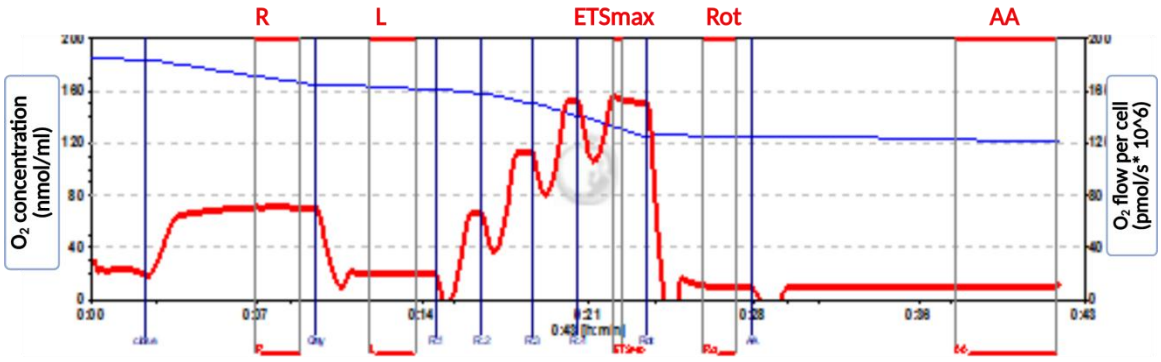

Image 15: Example of raw data obtained through OROBOROS oxygraph-2K.
The evolution of two slopes can be followed in time: the blue slope translates the O_2 concentration in the sample and the red slope corresponds to the O_2 flux per cell or cellular respiration. This graphic is a visual representation of the SUIT-003 protocol for living cells.
R=routine respiration without inhibitors or uncouplers; L= leak respiration after inhibition of ATP synthase with oligomycin; ETS_{max}= maximum potential respiration after incrementally adding an uncoupler (FCCP); Rot= respiration after inhibition of complex I with rotenone; aa= residual respiration after addition of antimycin a (inhibitor of complex III).

Once the chambers loaded with samples and closed with the stoppers, cells are allowed to do their normal metabolism in culture medium for about 5 minutes (R on Figure 15)(Image 14 A) after which 2µl oligomycin are added to inhibit ATP synthase and determine levels of the Leak respiration (L on Figure 15)(Image 14 B red cross). Oligomycin binds to ATP synthase at the level of the proton channel, which becomes unable to transport protons back to the matrix and to produce ATP. Therefore, it would be expected that O_2 consumption halts altogether.

However, some protons can leak through the inner mitochondrial membrane (Image 14 A, blue line), even during physiological conditions. This proton leak is responsible for the O_2 consumption that is still noticeable after inhibition of ATP synthase and is what we call leak respiration (Image 14 B, blue line). Leak respiration dissipates the proton gradient and decreases the energy that could be used for ATP synthesis. To put it in other words, leak respiration is linked to an oxygen consumption that does not lead to ATP production. It reflects a backflow of protons towards the matrix without passing through the ATP synthase (Ajit S Divakaruni *et al*,2011).

Continuing with the protocol, we incrementally add 2µl of FCCP (carbonyl cyanide-p-trifluoromethoxyphenylhydrazone) (Image 14 C green line) until we obtain the highest stabilization plateau. FCCP is a protonophore. It affects mitochondrial function by disrupting the coupling between ETC and OXPHOS, which makes it also an uncoupling agent. It is a weak acid that when found in highly acidic compartiments—such as the mitochondrial intermembrane space—binds to protons and translocates them easily through the inner mitochondrial membrane. Once in the matrix, where the pH is more alkaline, FCCP releases protons, thus collapsing the proton gradient. In other words, uncouplers allow the backflow of protons without limitations due to ATP synthase activity or membrane

impermeability. They are used to determine the ETS_{max} (ETS_{max} on Image 14 F or on Image 15) which represents the theorical maximum level at which ETC can function in order to replenish cells with ATP. Once the ETS_{max} plateau has been determined, 5µl of rotenone— a complex I inhibitor— are added (Image 14 D, yellow cross). Electrons cannot be extracted from NADH, resulting in less protons being concentrated in the intermembrane space and less oxygen consumed by complex IV. ETC function and O_2 consumption are only sustained by complex II and $FADH_2$ (Purple arrows on Image 14 D and Rot on Figure 15).

Finally, the addition of 1µl of antimycin a blocks complex III and allows to assess the part of oxygen consumption that is due to anything else but the mitochondria (Image 14 E, orange cross). By blocking complex III, site of convergence of all the extracted electrons, we block the translocation of electrons towards complex IV, which won't be able to combine O_2 with protons to form water. Any O_2 consumption detected at this point cannot be due to the mitochondrial respiration and is called residual respiration (AA on Figure 15).

2.3. Data treatment and interpretation

The raw data obtained can be expressed in terms of O_2 concentration (nmol/ml) (blue slope) or O_2 flux per cell (pmol/(s*million cells)(red slope) (Image 15).

O_2 flux basically reflects the O_2 consumption normalized to the number of cells in each chamber or in other words the oxygen consumption rate (OCR) for each cell.

Because mitochondrial content can vary through samples, representing a potential confounding factor for interpretations, it can be useful to normalize the results to citrate synthase activity. Citrate synthase is a Krebs cycle enzyme located in the mitochondrial matrix. Its activity correlates to the mitochondrial density of each sample. It can also be normalized to whole protein content, to account for possible cell number variations and to eliminate any confounding factor due to basal cellular metabolism or cell number accross samples.

In other words, the normalization of raw oxygraphy data to citrate synthase activity itself normalized to whole protein content allows to verify that the differences observed aren't due to any variations in mitochondrial content or cell number. It is a nested normalization for both cell number and mitochondrial density across samples (O_2 flux/cell/mitochondria).

The results obtained for routine and leak can also be represented as Flux control ratio (FCR) relative to ETS_{max}. Expressing the results as FCR allows to focus on functional quality and functional equilibrium between the different states.

For example, when taking the ratio Leak/ETS_{max} we can have an idea of the efficiency of ETC and OXPHOS coupling. An increased ratio means that there is a higher proportion of the total respiratory capacity that is not being used for ATP production, meaning that mitochondrial complexes are working to build a proton gradient that is wasted and not effectively used to produce ATP.
The same ratio can be done with Routine/ETS_{max} translating the part of the total respiratory capacity that is being used by cells routinely. This can show if, for example, a stress disturbs the basal metabolism of cells.

Hypothesis & strategies

Age-related diseases have been strongly linked to mitochondrial dysfunction and oxidative stress. Hydrogen Peroxide (H_2O_2) is a well described intracellular reactive oxygen species (ROS). Exogenous H_2O_2 can enter cells and their compartments through aquaporins, where it can follow several fates:
- it can be metabolized by the catalase into water and oxygen
-it can react with iron through the Fenton reaction producing other ROS
-it can oxidize macromolecules, particularly lipids and proteins containing iron-sulfur clusters
Despite this knowledge, there is currently limited to no research on how exogenous H_2O_2 affects mitochondrial function in living human muscle cells.
The objective of this thesis is to develop an *in vitro* model that mimics the oxidative context and mitochondrial dysfunctions that can be found in many age-related disease, including sarcopenia.
In order to do so, H_2O_2 is tested as a stress inducer on the LHCN-M2 cell line, which to our knowledge has not been tested before. The potential of H_2O_2 to induce a cellular stress is analyzed through MTS and CellTiter-Glo assays. Different parameters (H_2O_2 dilutions, incubation times, cell seedings) are tested in order to develop a standardized stress protocol on the LHCN-M2 cell line. Lastly but not least, the stress protocol is applied for analysis of mitochondrial function using High-Resolution Respirometry (HRR).
In this study, it was hypothetized that treatments with exogenous H_2O_2 will effectively induce an oxidative stress and, consequently, a mitochondrial dysfunction in human myoblasts (LHCN-M2 cell line), making it a relevant and useful *in vitro* model for the study of potential therapeutic strategies for mitochondrial or age-related diseases, such as sarcopenia.

Materials & methods

1. Cell line

We used the immortalized human myoblast cell line LHCN-M2 (abm, Canada) as a model for human skeletal muscle tissue. This cell line has been genetically modified to express hTERT and cdk4 to enable proliferative capacity. Expressing hTERT allows to bypass cellular senescence due to the shortening of telomeres while the expression of cdk4[3] prevents senescence due to stress, often observable in vitro, such as confluence.

2. Cell culture of LHCNM2

Cells are maintained in a medium composed of DMEM high glucose (BioWest, France) and Medium 199 (VWR, Belgium) (4:1) supplemented with 15% of heat inactivated FBS; 1.4µg/ml of vitamin B12 (Merck, Germany); 0.055µg/ml of dexamethasone (TCI, Europe); 0.03µg/ml of zinc sulfate heptahydrate (Merck, Germany); 0.02M of HEPES (BioWest, France); 10ng/ml of FGF_2 (StemCell Technologies, France); 2.5ng/ml HGF (StemCell Technologies, France) and 1% of penicillin/streptomycin (BioWest, France), according to the manufacturer's advice.

Cells are maintained at 37°C in a 5% CO_2 cell culture incubator and passed each three days.

3. Stress model in microplate

We treated LHCN-M2 cells cultured in microplate with different H_2O_2 concentrations.

LHCNM2 cells were seeded at 15000 cells per well on a total volume of 100µl and let adhere overnight (never more than overnight otherwise cell population might double).

Cells are rinsed with 100µl of HBSS 1x (Gibco 14025-050; Life Technologies, US) before charging the conditions in order to eliminate traces of culture medium and get more reproductible results.

The H_2O_2 stock solution (Suprapur Hydrogen Peroxide 30%; Merck, Germany) was diluted 100-fold in HBSS to prepare a 0.1M mother solution, from which serial dilutions were performed to obtain the desired concentrations. The true molarity of the stock solution was calculated to be approximately 9.8M, but was rounded to 10M to simplify calculations.

The cells were exposed to the H_2O_2 concentrations and the controls (HBSS and culture medium) for 1h at 37°C on a total volume of 100µl per well.

4. Assessment of stress efficiency using MTS assay

To evaluate the quality of the stress we use the MTS (ProMega CellTiter96® AQueous One solution Cell proliferation assay).

---

[3] Cdk4 forms a complex with cyclin D to phosphorylate pRb leading to its inactivation and liberation of E2F transcription factor, while in turn allows for the progression of the cell cycle towards S phase.

MTS solution was prepared by mixing the solution containing the tetrazolium salt with the PES-containing solution. The mix was aliquoted and stored at -20°C to avoid freeze-thaw cycles.
For adherent conditions, cells were incubated for 1h (or 2h) at 37°C with the stress conditions and controls (HBSS and culture medium), we washed each well with 100µl of HBSS 1x to eliminate traces of H_2O_2.
Another 100µl of HBSS were added followed by 10µl of MTS mix to each well.
Signal was monitored using a spectophotometer (Multiskan Ascent, Labsystems) at 492nm.
Measures were saved at two time points, at T0 and at T3h. T0 allows the measurement of background noise. Subtraction of T0 from T3h values allows the extraction of real values of formazan formation.
For cells in suspension, after the treatment, cells were detached and collected in HBSS, counted and diluted with HBSS in order to obtain 15000cells/well in 100µl. Then 10µl of MTS mix was added to each well and measurements were performed are mentioned herein above.

5. Estimation of IC50

Please "To estimate IC50, experiments using MTS or CellTiter-Glo assay were performed. The resulting data were analyzed using Quest Graph™ IC_{50} calculator from AAT Bioquest Inc, which applies a four-parameter logistic regression model (https://www.aatbio.com/tools/ic50-calculator).
This online tool allows users to input the concentrations under study along with the corresponding replicates, generating both numerical estimates and graphical representations of the dose-response curve.

6. Transposition of the stress protocol to bigger culture surfaces

The standardized protocol for the H_2O_2 was established on microplate.
15000 cells on 0.32cm^2 are equivalent to 3.5 10^6 cells on T75 (75cm^2).
The H_2O_2 availability ratio was also defined but not respected for the oxygraphy testings (only 10ml of total stress volume) (see Results for explanations).
3.5 10^6 cells were let to adhere overnight to T75 flasks. The next day we added a total stress volume of 10ml containing different H_2O_2 concentrations (diluted in HBSS) and controls. For negative controls we incubated cells with 10ml of culture medium (Mi) or with 10ml of HBSS (buffer used to dilute the H_2O_2 stock solution).
Cells were incubated for 1h with the different conditions at 37°C.
Then, each T75 flask was washed with 5ml of PBS (to eliminate traces of calcium in culture medium and HBSS, which might affect the activity of trypsin); 2ml of synthetic trypsin (Tryple express, Gibco) were

added to each flask for 5min at 37°C for optimal activity. Trypsin was inactivated by adding 6ml of PBS to each flask.

Lastly, cell suspension was collected on a sterile falcon of 15ml and centrifuged at 130g for 5 minutes. Cell pellet was isolated and resuspended in 1ml of culture medium for oxygraphy analysis or 1ml of HBSS for CellTiter-Glo or MTS assays. Either way, 10µl of cell suspension was used to count the number of cells using a microscope and a Bürker counting chamber.

7. Measurement of ATP content using CellTiter-Glo assay

We used CellTiter-Glo assay (Promega) to evaluate how the H_2O_2 affected ATP production.

CellTiter-Glo is a chemiluminescent assay that relies on the activity of luciferase which needs ATP to allow luciferin to be oxidized by O_2 and to convert it to oxyluciferin.

Chemiluminescence was analyzed using a fluoroscope (Fluoroskan FL, Labsystems).

After cells were cultured on T75 flasks, trypsinized and counted, we added 50µl of cell suspension containing 15000 cells to each well and completed the volume with 50µl of CellTiter-Glo mix.

Analysis was done immediately after adding the mix. Measures included T0 for background noise, followed by 3 other measures, 5min apart for kinetic measurements. Each measure was intercalated with shakes to homogenize the wells. We substracted T0 values to the highest measure obtained usually (T3).

For cells in suspension, after the cells were treated with the different conditions, they were detached and collected in HBSS, counted and diluted with HBSS in order to obtain 15000 cells/well in 50µl. Then 50µl of CellTiter-Glo mix was added to each well and luminescence measurement was performed as mentionned above.

8. Analysis of mitochondrial respiration using oroboros high-resolution respirometry

Respiration was measured using Oroboros oxygraphs for high-resolution respirometry. Total chamber volume was set at 2ml at 37°C. DatLab software (Oroboros Instruments, Innsbruck, Austria) were used for data acquisition and analysis.

We opted for the oroboros SUIT-003[4] (MiPNet08.09) protocol for real-time OXPHOS analysis for living cells with a minimum of one million cells per chamber.

Following calibration of the chambers with 2mL of culture medium to determine background interference, each oxygraph was loaded with at least one million cells per condition per chamber.

Each condition was split into two chambers and measured in parallel as technical repeats.

The initial measurements of oxygen consumption of cells in the medium corresponds to the physiological

[4] **SUIT-003 (Substrate-uncoupler-inhibitor-titration)**

respiration (routine respiration), without inhibitors or substrates. After 15-30 minutes, if routine levels were stabilized, 2µL of oligomycin were added to each chamber (1µg/ml final concentration). When a novel steady state was reached, 2µL of FCCP were also added (1µM final). FCCP should be administered incrementally until the stabilization plateau begins to decline. Subsequently, 5µL of rotenone (0.5µM final) were added, followed by 1µL of antimycin A (0.5µM final) a couple of minutes later.

Each stabilization plateau after the addition of oligomycin, FCCP, rotenone, antimycin A has a metabolic meaning. Explanations can be found in the introduction chapter and complemented in the result, conclusions and discussion sections.

Raw oxygraphy data was corrected for residual respiration (subtraction of respiration values after antimycin A was added), normalized to citrate synthase activity itself normalized to whole protein content. Results were exposed as raw O_2 flux to analyze general trends or as Flux Control Ratio (controlled for ETS_{max}) for analysis of respiration efficiency.

9. Normalization of mitochondrial respiration with citrate synthase assay

We used Cayman chemical's MitoCheck citrate synthase activity assay kit (701040) for the quantification of citrate synthase and followed the manufacturer's protocol.

Citrate synthase was normalized according to whole protein dosage and used as a way to normalize mitochondrial content and cell count within samples.

After following the protocol for stress application on T75 flasks (number 6 of Materials & Methods), when cells are trypsinized, centrifuged and the cell pellet collected and resuspended in 2ml of culture medium for oxygraphy readings (number 8 of Materials & Methods), a small amount of cell suspention is preserved for citrate synthase activity assay. Citrate synthase is the first enzyme of the Krebs cycle. It catalyzes the following reaction:

$$\text{Oxaloacetate} + \text{acetyl coA} \rightarrow \text{Citrate} + \text{Coenzyme A (CoA} - \text{SH)}$$

The kit contains the assay buffer, oxaloacetate reagent, acetyl-coA reagent, a developer reagent and a positive control.

The developer reagent reacts with CoASH creating an yellowish compound. The absorbance of this compound is measured at 412nm. The slope of the plot absorbance(y axis) vs Time (x axis) in used to calculate enzyme activity (reaction rate).

$$\left(\frac{reaction\ rate}{5.712 mM^{-1}} \times \frac{0.1ml}{0.03ml}\right) \times sample\ dilution = \mu mols/min/ml$$

(Equation from Cayman's MitoCheck Citrate Synthase Activity assay Kit 701040)

10. Analysis of ROS production

We used Sigma Aldrich H_2DCFda ROS probe (MW: 487.29g/mol).

H_2Dcfda probe is initially non-fluorescent and enters the cell where it undergoes a deesterefication. It is when the DCF is oxidized by ROS that it becomes fluorescent (λEx/Em: 504/524nm).

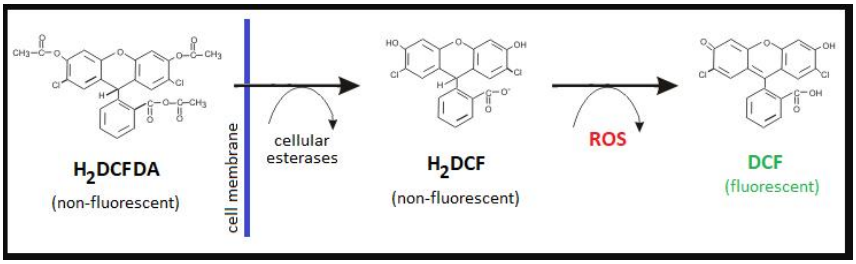

Image 16: Mechanism of H_2DCFda fluorescence for ROS analysis (Nova Z *et al*, 2020).

To aliquot a 10^{-3}M solution, 3.3mg of the probe were weighted and diluted in 6.77ml of ethanol.

3.5 million cells were seeded on T75 flasks and let adhere overnight. The following day, stress protocol on T75 flasks was applied. Cells were incubated with the different stress conditions, which included cells on culture medium or HBSS 1h/2h as negative controls, and cells incubated with different H_2O_2 concentrations (0.25mM 1h/2h, 0.4mM, 0.7mM). After rincing the flasks with PBS (5ml), detaching the cells with tryple E(4ml), which was inhibited by adding PBS (6ml), cell suspensions were collected on 15ml falcons and centrifuged at 130g for 5 minutes. The cell pellet was resuspended on 1ml of HBSS and the cells were counted using a Bürker counting chamber. Cell solutions were diluted in HBSS in order to obtain 15000 cells per 100µl. 100µl of cell suspension were added to a transparent microplate on 6 replicates per condition. 1µl of H_2DCFda solution was added to each well and incubated for 30 min at 37°C in the dark.

11. Evaluation of cell death using sytox green

Sytox green stain is a high-affinity nucleic acid stain that does not cross the membranes of live cells. However, in dead cells or cells with compromised membranes, it enters and binds to DNA and RNA producing a bright green fluorescence (λex/em: 504nm/523nm).

Sytox green was used to perform a manual counting of cell death. For this experiment, another microplate was seeded with 15000 cells per well and let adhere overnight. Cells were washed with HBSS and incubated for 1h with 100µl of culture medium or HBSS or different H_2O_2 concentrations (0.1mM, 0.2mM, 0.25mM, 0.4mM, 0.7mM, 1mM). After 1h, cells were washed with HBSS and 100µl of 170µM Sytox green solution was added. After 10 minutes, 100µl of Hoechst solution in HBSS (5µg/ml) (InVitrogen) was also added to the wells. Hoechst is a cell permeable nucleic stain that emits blue fluorescence (λex/em: 350nm/461nm). After 10 minutes of incubation with hoechst, the fluorescent signals were observed under a fluorescent microscope using an excitation filter 450-490nm for green

fluorescence and 360nm for blue fluorescence. Pictures from 2 different fields under the microscope were taken with each filter. The counting of the cells was performed with ImageJ by adjusting pixel size between 200 to 25000 and circularity from 0.3 to 1.

12. Evaluation of cell viability using trypan blue

Cells were cultured on T75 flasks according to the transposition protocol (3.5 milion cells per T75 flask using 10ml of total stress volume).

Cells were let to adhere one overnight and the following day they were rinsed with HBSS (5ml) as well as charged with the different experimental conditions (Cells in culture medium or HBSS 1h and 2h; 0.25mM, 0.4mM, 0.7mM of H_2O_2 1h; 0.25mM of H_2O_2 2h). After incubation, the flasks are rinced with PBS (5ml) and tryple Express (4ml) is added for 5 min at 37°C. After verifying that cells were well detached, they were collected into a 15ml falcon tube for each condition, to which we added PBS (6ml) to inhibit trypsin's activity. Cells were centrifuged at 130g for 5 minutes and cell pellet was resuspended in 1ml of culture medium.

In an eppendorf tube we added 10µl of cellular suspension, 190µl of culture medium and 50µl of trypan blue. 10µl of the mix was used on a Burker counting chamber. Total number of cells was counted as well as the cells marked by trypan blue for evaluation of cell mortality. These numbers were multiplied by 25 (dilution in the eppendorf tubes) and by 10000 to obtain numbers per milliliter of cell suspension.

Statistical Analysis

Statistics were done using GraphPad Prism 8.0.2.

Normality was checked for every sample in every graphic.

If normality was confirmed, a one-way ANOVA followed by multiple comparisons post hoc test was done.

If normality was not confirmed, a non -parametric Kruskal-Wallis test was used followed by a post hoc test for multiple comparisons.

Details about the normality and utilized tests are given below each figure, along with symbols for p-values.

Results

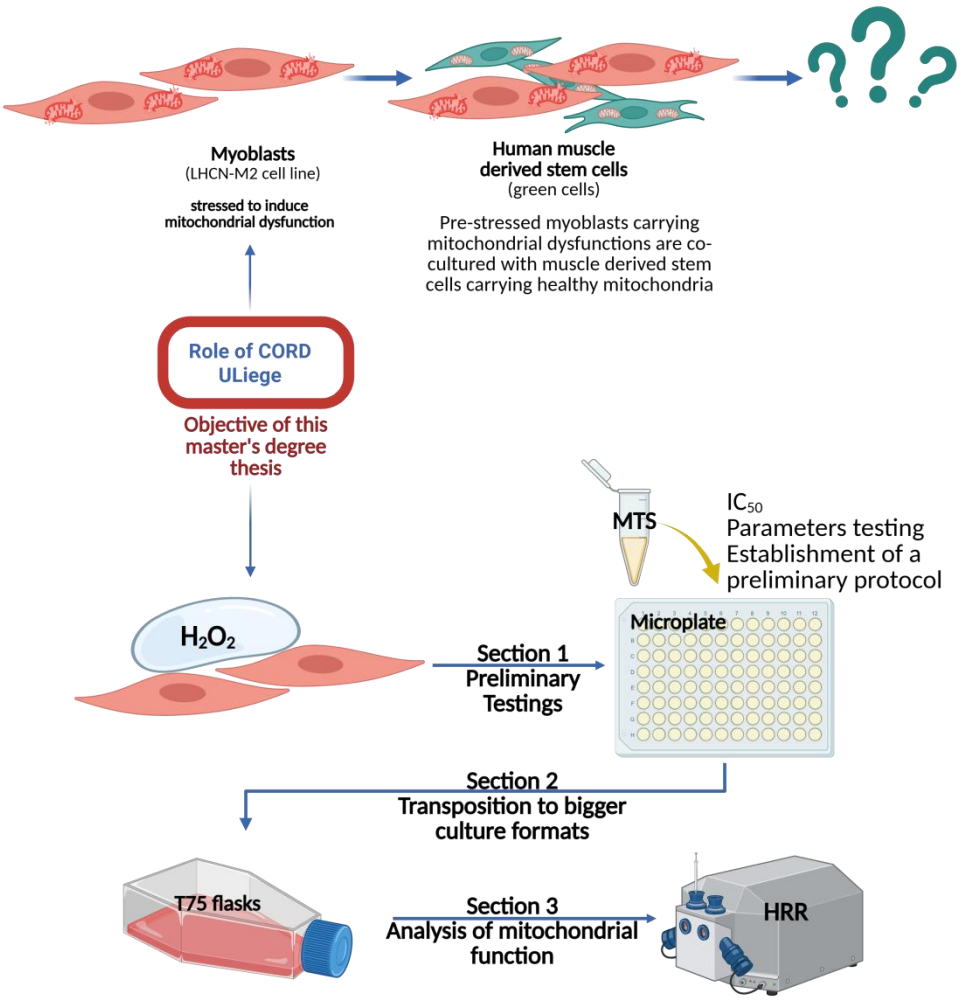

Image 17: Overview of the scientific strategy of this master's degree thesis and the workflow of the results section

The results chapter is divided into three sections (Image 17).

The first section of the results, was dedicated to the identification of parameters that interfered with the quality of the H_2O_2 stress perceived through the MTS assay readouts. The main goal was to establish a preliminary protocol to guarantee standardized experimental conditions.

We also determined the IC_{50}, defined as the concentration of H_2O_2 at which the MTS signal is reduced to 50% of that observed for the negative control—typically the buffer used to prepare H_2O_2 dilutions (HBSS).

The second section of the results is dedicated to the transposition of the preliminary stress protocol to larger culture formats—a necessary step in order to be able to perform robust high-resolution respirometry (HRR) measurements, which require an important number of cells.

Last but not least, the third section of the results was dedicated to high-resolution respirometry results.

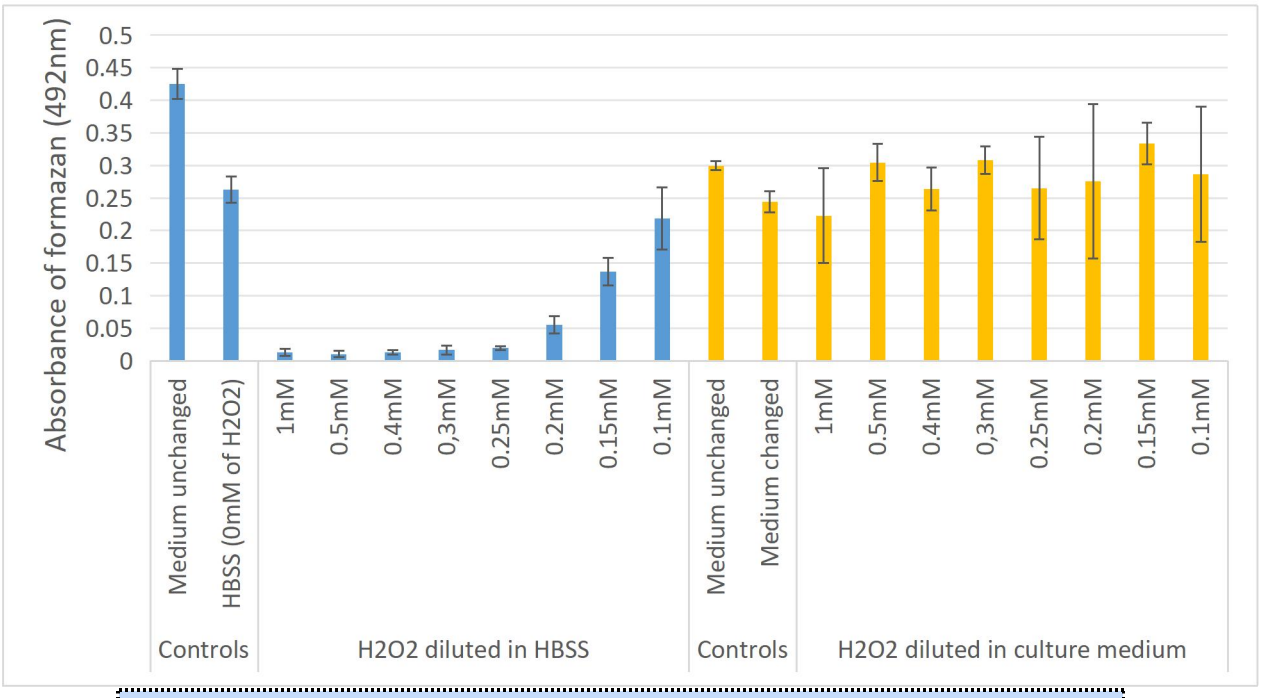

Figure 1: MTS assay performed in 96-well plate using 10000 cells per well.

H_2O_2 was diluted in either culture medium (orange bars) or HBSS (blue bars) at concentrations ranging from 1mM to 0.1mM in a total volume of 100µl per well. Cells were incubated for 1h at 37°C prior to analysis.The "medium unchanged" control refers to cells that remained in the same culture medium used for the overnight incubation. In contrast, the "medium changed" control refers to cells that received 100µl of fresh culture medium.

Mean ± SD from one independent experiment with 8 total technical replicates for each condition.

1. Development of a standardized exogenous H_2O_2-induced stress on the LHCN-M2 cell line

Initial testings were conducted on 96-well plates in order to optimize the screening of several H_2O_2 concentrations. The primary goal of this result section is to identify the key parameters that can affect how the H_2O_2 stress is perceived by cells, as measured through the MTS assay.

1.1. Effect of the dilution of H_2O_2 in culture medium or HBSS:

For the dilutions of H_2O_2, two different solvants were considered: HBSS or culture medium. HBSS is usually a good replacement for PBS, as it contains essential ions (calcium and magnesium) and buffering agents (bicarbonate) (Katori R *et al*, 2016). Different H_2O_2 dilutions were tested in either culture medium or HBSS in 96-well plates at 10000 cells per well and incubated for 1h at 37°C (Figure 1).
Based on these results, we concluded that when diluted in the culture medium, H_2O_2 likely had a short half-life or its negative effect was counteracted by the positive effect of culture medium on cellular metabolism (Fan X *et al*, 2010). Indeed, the presence of nutrients in the medium may mitigate the stress, resulting in a less pronounced effect as detected through MTS assay readouts after only one hour of exposure to hydrogen peroxide. Diluting H_2O_2 in HBSS not only decreased cell metabolism (blue bars, comparison between medium unchanged and HBSS controls) but also allowed to obtain a dose-dependent effect of the H_2O_2.
From these preliminary tests, it was decided that H_2O_2 dilutions should be prepared using HBSS as the solvent, as it induced a dose-dependent response to the stress.

1.2. Effect of the initial seeding:

Since MTS assay indirectly measures the metabolic activity of cells, we evaluated how the number of cells per well (seeding) affected readouts.
LHCN-M2 cells were seeded at varying densities (10000, 15000, 20000 and 25000 cells/well) and incubated for 1h at 37°C with H_2O_2 diluted in HBSS at concentrations ranging from 0.1mM to 1mM.
As shown in Figure 2, the H_2O_2 concentrations affected cellular metabolism in a dose-dependent manner for each seeding density but exhibited a stronger effect on the lower seedings, indicating that for higher seeding densities, the IC_{50} shifted towards higher H_2O_2 concentrations.
Relying on these results, it was decided to proceed with an initial seeding of 15000 cells per well ($0.32cm^2$) for the subsequent experiments. At this seeding density, the IC_{50} is estimated to be situated between 0.20 and 0.25mM of H_2O_2 (according to AAT Bioquest).

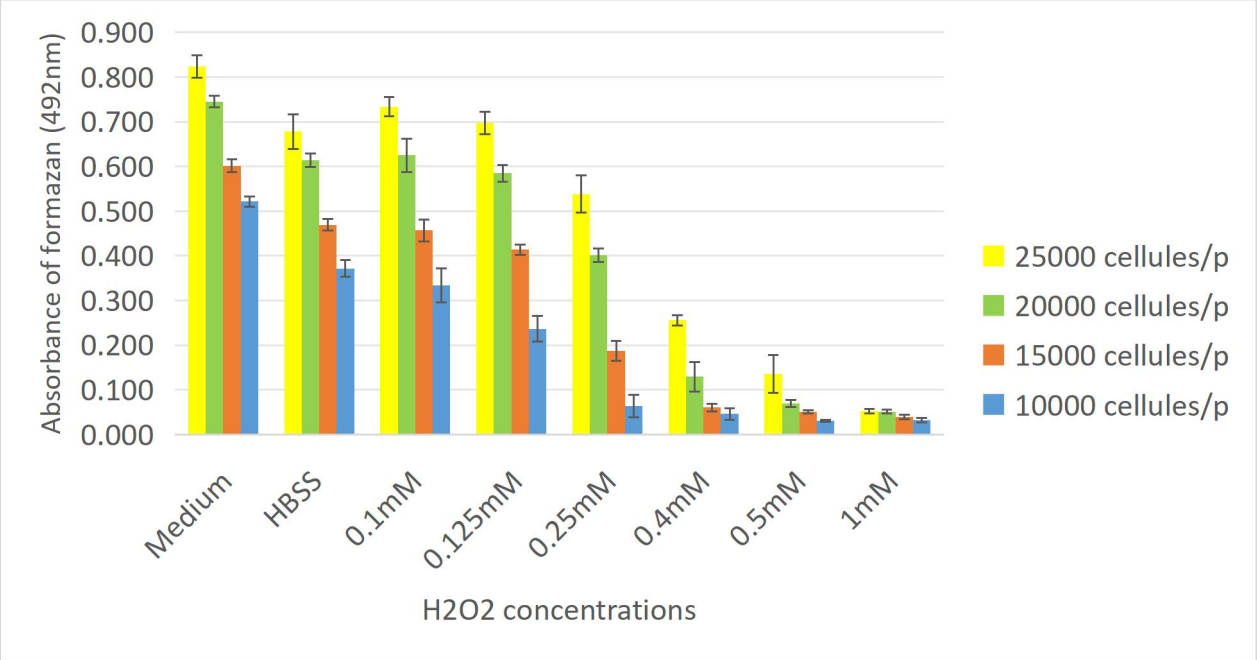

Figure 2: Effect of the exogenous H_2O_2 (0.1mM-1mM) on different seeding densities using MTS assay.

Wells on a 96-well plate were seeded with 10000, 15000, 20000 and 25000 cells per well. The cells were incubated with the different conditions (H_2O_2 concentrations ranging from 0.1mM to 1mM and negative controls cells incubated with culture medium or HBSS) in a total volume of 100µl for 1h at 37°C prior to analysis

Mean ± SD from two independent experiments with 3 total technical replicates for each condition for each experiment.

1.3. Effect of the incubation time:

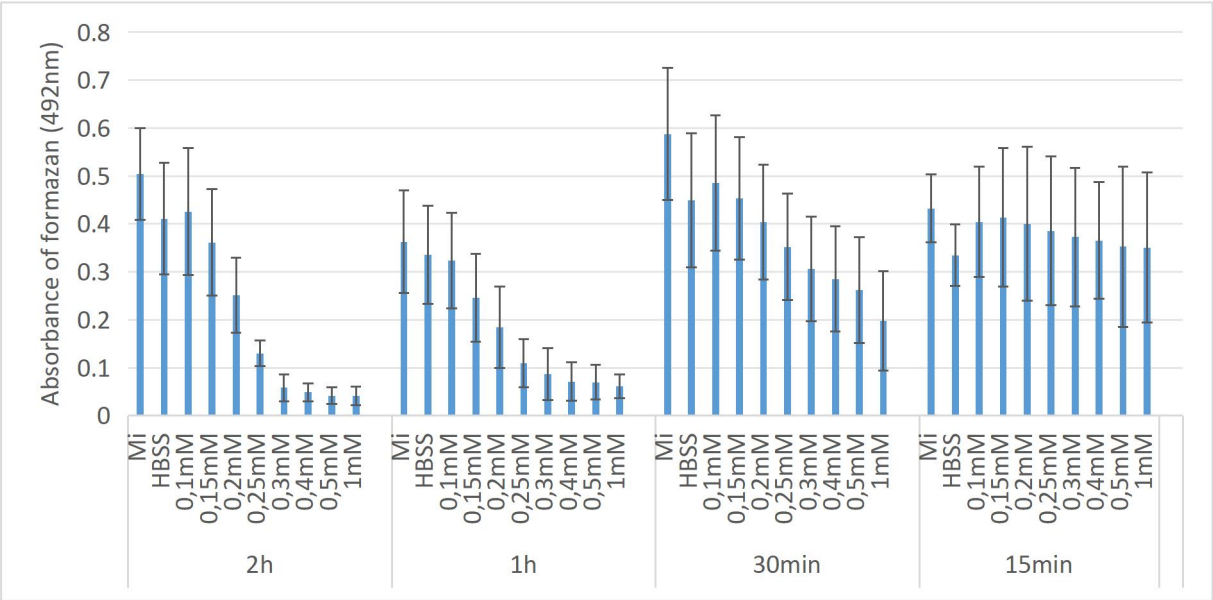

Figure 3: Testing different incubation times with 15000 cells per well using MTS assay.

Cells were treated with the different H_2O_2 concentrations (0.1mM to 1m) and incubated for 2h, 1h, 30minutes or 15 minutes at 37°C.

Mean ± SD from three independent experiments with a total of 4 technical replicates per condition per experiment.

The next logical parameter to test was the incubation time to see how it affected the MTS assay readouts. As shown in Figure 3, 15 and 30 minutes of exposure to H_2O_2 did not appear to be sufficient to induce a dose-dependent response. A dose-dependent response appeared to be more marked with incubation times of 1h and 2h, but the 1h of incubation appeared to decrease progressively with the increasing H_2O_2 concentrations. At 2h of incubation, the inhibitory response appeared to be similar between 0.3mM and 1mM.

Moreover, 1 hour of incubation with the stress may reduce excessive cellular stress or damage which could occur with longer exposures, while also eliminating external confounding factors, such as nutrient depletion or byproduct accumulation (Figure 1 comparison between medium and HBSS controls), which could interfere with the interpretation of the results.

Upon these initial testings, a preliminary stress protocol was established as follows:

-15000 cells per well (0.32cm^2)

-1 hour of exposure to H_2O_2 concentrations or control conditions

-H_2O_2 should be diluted using HBSS as the buffer.

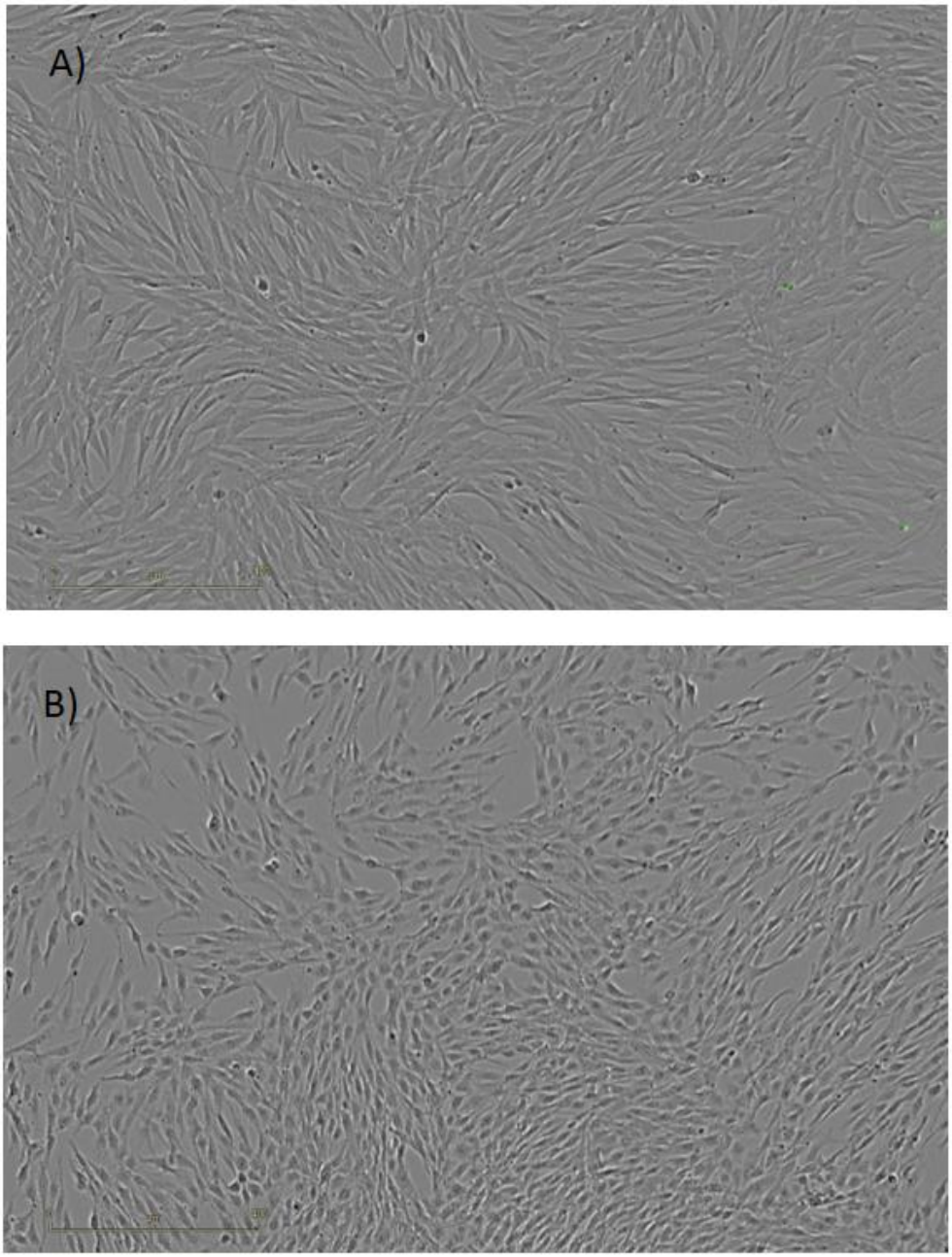

Image 18: Picture taken by the incucyte device of LHCN-M2 cultured in 96-well plate after 1h of experiment.

A) Morphology of cells treated with HBSS after 1h of incubation

B) Morphology of cells treated with 1mM of H_2O_2 after 1h of incubation

Bar: 400µm

1.4. Effect of the exogenous H_2O_2 on cellular viability

MTS assay is widely used as a viability assay. Slowed formazan formation can therefore be associated with cell death. To ensure that the decrease in signal observed with the MTS assay was not due to an increase in cellular death, we used Sytox Green and Hoechst stainings. Sytox green is a specific nucleic acid stain which emits green fluorescence upon binding to nucleic acids. Hoechst dye, also a nucleic acid dye, emits blue fluorescence when bound to DNA. The key difference between these two is their ability to cross cell membranes: Hoechst dyes are cell-permeable and stain the nuclei of both live and dead cells, whereas Sytox Green is impermeable to live cells and only enters the cells that have a compromised plasma membrane. Mortality was calculated by the ratio between the number of nuclei in dead cells stained with Sytox Green to the total number of nuclei stained with Hoechst from the same field. In total, two different microscope fields were photographed for each condition to calculate the ratio (Table 1).

Conditions	% Cell mortality (Mean ± SD)
Milieu	7.4 ± 2.1
HBSS	7.0 ± 5.5
H_2O_2 (0.1 mM)	3.7 ± 0.6
H_2O_2 (0.2 mM)	5.5 ± 0.5
H_2O_2 (0.25 mM)	4.9 ± 2.0
H_2O_2 (0.4 mM)	5.7 ± 1.0
H_2O_2 (0.7 mM)	6.0 ± 0.7
H_2O_2 (1 mM)	5.5 ± 2.0

Table 1: Determination of cell mortality of LHCN-M2 exposed or not during 1h of exposure to several H_2O_2 concentrations. Nuclei of dead cells were stained with Sytox Green while nuclei of every cell were stained with hoechst.
Mean ± SD from 3 independent experiments.

The results summarized in Table 1 showed that H_2O_2-treated cells did not exhibit higher cellular toxicity compared to untreated cells in medium and in HBSS. Under all conditions, the average cellular toxicity remained under 10%.

Moreover, by using Incucyte System for Live Imaging from Giga-Cell Imaging platform, we were also able to demonstrate that there was no significant cellular detachment within the 1h of treatment (Image 18), only a slight modification of the cell structure observed for high H_2O_2 concentrations. Indeed, the cells appeared thinner, with a higher contrast, making the outlines of the nuclei more visible.

These experiments were important to determine that the previous results obtained throught the MTS assay (MTS readouts decrease in a dose-dependent manner with increasing H_2O_2 concentrations) cannot be explained by an increase in cellular death.

2. Transposition of the stress protocol to larger culture formats (T75 flasks)

Once the parameters which can affect reproducibility of the stress on microplate have been identified and a standardized protocol has been established, this protocol had to be adapted for use in larger culture formats (T75 flasks) to ensure sufficient cell collection for the continuation of the project. Indeed, high-resolution respirometry experiments using oroboros oxygraphs requires at least one million cells per chamber per condition in order to obtain stable and reliable data.

There are a couple of parameters that obviously needed to be adapted to larger culture formats: the seeding density and the stress volume.

The surface area of a well in microplate is approximately 0.32cm^2. To maintain the same seeding density per area unit, T75 flasks (75cm^2) must be seeded with 3.5 10^6 cells.

$$\frac{15000\ cells\ (chosen\ ideal\ seeding)}{0.32cm^2\ (area\ of\ well\ on\ microplate)} \times 75cm^2 (area\ of\ T75\ culture\ flasks) \cong 3.5\ million\ cells$$

Regarding the volume of stress, on microplate, the total stress volume was 100µl, which is also the volume to allow cell adhesion overnight. However, 100µl for 15000 cells in microplate is equivalent to approximately 23.5ml to a total of 3.5 10^6 cells in T75 flasks.

$$\frac{100\mu l}{15000\ \text{cells}} = 6.7 \times 10^{-3}\mu l\ \text{per cell} = 0.0067\mu l\ \text{per cell}$$

$$\frac{x}{3500000\ \text{cells}} = 0{,}0067\mu l\ \text{per cell} \leftrightarrow x = 0{,}0067\mu l \times 3500000 = 23450\mu l = 23{,}450ml$$

$$\frac{Total\ stress\ volume}{Total\ cell\ count} = H_2O_2\ availability\ ratio$$

The total stress volume relative to the total cell count is a crucial parameter, as it translates the availability of H_2O_2 molecules or a total number of H_2O_2 molecules per cell.

This way, for a complete transposition of the stress to T75 flasks, the conditions required were:

-overnight adhesion of 3.5 10^6 cells

-total stress volume of 23.5ml

-1h of incubation with the stress conditions or controls

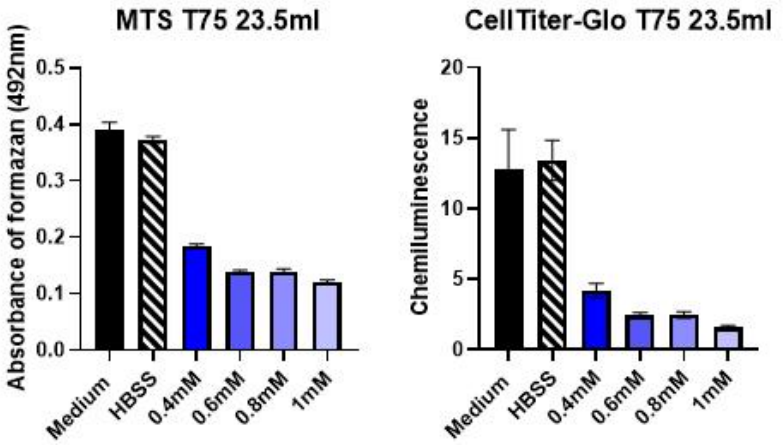

Figure 4: Estimation of the IC_{50}, through MTS and CellTiter-Glo assays, on T75 flasks respecting the volume for the right H_2O_2 availability ratio (23.5ml). Blue bars correspond to samples treated with different H_2O_2 concentrations.
Mean ± SD from one independent experiment with 5 technical replicates for each condition.

As it was depicted in Figure 4, when all of the parameters above-mentionned were respected, the same IC_{50} was estimated in T75 flasks, both using MTS and CellTiter-Glo assays. AAT Bioquest estimated an IC_{50} at about 0.2799mM using the MTS assay and at 0.2332mM with the CellTiter-Glo assay for the same cell samples (roughly the same IC_{50} (0.25mM) estimated on microplate).
The results from Figure 4 confirmed a successful translation of the preliminary protocol to a larger culture surface. These results also demonstrated that the use of CellTiter-Glo assay (20 minutes) yielded comparable outcomes to the MTS assay (4h of incubation). This finding was particularly valuable, as it showed that CellTiter-Glo assay could be used as an alternative to evaluate the effectiveness of the stress.

Despite the successful translocation of the preliminary protocol to larger culture formats, it was decided that, for the continuation of the project, the H_2O_2 availability ratio would not be respected as it was preferable to rather work with the volume for cell adhesion (10ml), since using 23.5ml per T75 flask was deemed wasteful.

	Parameters	Mathematical calculation of H_2O_2 availability ratio taking into account H_2O_2 molarity
A) 0.25mM using microplate parameters	100µl of total stress volume 15000 cells per well 0.25mM of H_2O_2	$\frac{2.5 \times 10^{-3}\text{moles} \times 100 \times 10^{-6}\text{L}}{1\text{L} \times 15000\ \text{cells}}$ $= 1.67 \times 10^{-12}\ \text{moles of}\ H_2O_2/\text{cell}$
B) 0.25mM using T75 respecting every parameter	23.5ml of total stress volume 3.5 10^6 cells 0.25mM of H_2O_2	$\frac{2.5 \times 10^{-3}\text{moles} \times 23.5 \times 10^{-3}\text{L}}{1\text{L} \times 3.5 \times 10^{6}\text{cells}}$ $= 1.68 \times 10^{-12}\ \text{moles of}\ H_2O_2/\text{cell}$
C) 0.25mM using T75 not respecting the right volume	10ml of total stress volume 3.5 10^6 cells 0.25mM of H_2O_2	$\frac{2.5 \times 10^{-3}\text{moles} \times 10 \times 10^{-3}\text{L}}{1\text{L} \times 3.5 \times 10^{6}\text{cells}}$ $= 7.14 \times 10^{-13}\ \text{moles of}\ H_2O_2/\text{cell}$
D) Estimation of new IC_{50} on T75 with 10ml of total stress volume	10ml of total stress volume 3.5 10^6 cells x mM of H_2O_2	$\frac{\text{x moles} \times 10 \times 10^{-3}\text{L}}{1\text{L} \times 3.5 \times 10^{6}\text{cells}} = 1.67 \times 10^{-12}\ \text{moles of}\ H_2O_2/\text{cell}$ $\leftrightarrow \text{x} = \frac{1.67 \times 10^{-12}\text{moles of}\ H_2O_2\ /\ \text{cell} \times 1\text{L} \times 3.5 \times 10^{6}\text{cells}}{10 \times 10^{-3}\text{L}}$ $\leftrightarrow \text{x} = 5.8 \times 10^{-4}\text{moles of}\ H_2O_2 = 0.58\ \text{mmoles of}\ H_2O_2$

Table 2: Comparison of H_2O_2 availability ratio variations translated as H_2O_2 moles per cell.

A) Parameters used for preliminary tests on microplate and IC_{50} concentration determined by AAT Bioquest
B) Parameters were transposed to T75 flasks culture surface, respecting the number of cells per square centimeter and the total stress volume per cell
C) Total stress volume for T75 flasks was not respected (wanted working volume of 10ml)
D) Estimation of the new IC_{50} applying the wished working volume

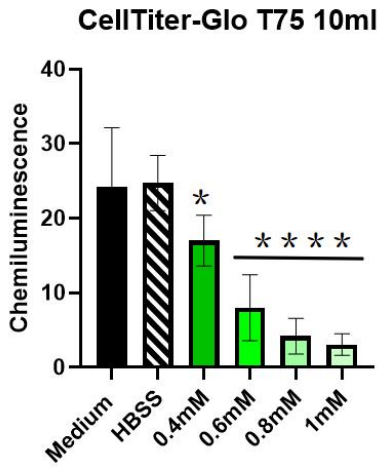

Figure 5: Estimation of the functional IC_{50}, through CellTiter-Glo assay, on T75 flasks using only 10ml of total stress volume. Green bars correspond to samples treated with different H_2O_2 concentrations.
Mean ± SD from five independent experiments with a total of 4 technical replicates for each condition for each experiment.
Normality was verified but not respected. A Kruskal-Wallis test was performed ($p<0.0001$) followed by a Dunn's test for multiple comparisons.
HBSS control was compared to Medium control. All the H_2O_2-treated samples were compared to the HBSS control.
(* $p<0.05$; * * $p<0.01$; * * * $p< 0.001$, * * * * $p<0.0001$)

The H_2O_2 availability ratio can also be expressed as moles of H_2O_2 per cell (Table 2).
For the experiments conducted in microplate (Table 2 A), H_2O_2 availability was calculated for the IC_{50} concentration (0.25mM). When all the parameters were carefully adapted to the T75 flasks (Table 2 B), the same H_2O_2 availability per cell was obtained ($1.68x10^{-12}$ moles of H_2O_2 per cell). These results (Table 2 A and B) further confirmed a favorable translocation of the stress protocol to larger culture formats.
The same calculations were applied taking into account the intended working volume of 10ml (Table 2 C), for which the H_2O_2 availability per cell decreased, indicating that a higher H_2O_2 concentration would be necessary in order to get the IC_{50}. Subsequently, the same approach was used to estimate the H_2O_2 concentration required to achieve the IC_{50} for a working volume of 10ml (Table 2 D) (0.58 mM of H_2O_2).
To verify these estimations, a CellTiter-Glo assay was performed using a total stress volume of 10ml (Figure 5). Under these conditions, *ceteris paribus*, the IC_{50} was estimated to be approximately 0.45mM (according to AAT Bioquest).

The theoretical IC_{50} derived from the H_2O_2 availability ratio (Table 2 D) did not align with the actual functional IC_{50} determined using Celltiter-Glo assay data (Figure 5), creating a discrepancy that challenged the empirical determination of the IC_{50}.
To account for this variability, three H_2O_2 concentrations— 0.25mM, 0.4mM and 0.7mM— were selected for high-resolution respirometry measurements. This approach made it possible to encompass the response range between the functional and theoretical IC_{50s} (0.4mM is slightly below the functional IC_{50} and 0.7mM is slightly above the theoretical IC_{50}).
To summarize, 0.25mM enables the assessment of sublethal effects, 0.4mM approximates the functional IC_{50} as determined by ATP content measurements and 0.7mM exceeds the theoretical IC_{50} estimated from the H_2O_2 availability ratio allowing for the evaluation of more severe effects.

3. Effect of exogenous H_2O_2-induced stress on mitochondrial function of LHCN-M2 cells

Since the goal of the H_2O_2 stress was to hopefully induce mitochondrial dysfunction— one of the hallmarks of sarcopenia— it was necessary to assess how this stress affected the mitochondrial respiration in LHCN-M2 cells using High-Resolution Respirometry (HRR).

As detailed on the Material & Methods section, we followed the SUIT-003 protocol for living cells (Oroboros instruments) (Eric Gnaiger *et al*, 2012). This protocol requires the use of inhibitors, uncouplers or substrates that are naturally permeable to intact cells. While this approach presents some limitations, it allows us to preserve near-physiological conditions (cells are alive in the culture medium, are neither fixed nor permeabilized and no mitochondrial isolation is required).

Before using the cells in HRR, several parameters were studied after cell detachment with trypsin: cell counting to check an eventual loss of cell after H_2O_2 treatment, the cell mortality using blue trypan exclusion test (Table A1 Appendix), cell morphology by inversed microscope, and cell metabolism parameters as studied for adherent cells (Image A1 Appendix). Overall,the collected cell number remained relatively similar across samples and mortality remained under 5% of the total cell count. These results demonstrate that the cells inserted into the chambers were predominantly alive. However, as portrayed in Image A1, cells treated with H_2O_2 reacted different to trypsination and exhibited a post-detachment fusiform phenotype that increased in frequency with the H_2O_2 concentration.

3.1. High-Resolution Respirometry (HRR) for mitochondrial analysis:

When it comes to mitochondrial function, the general trend that could be extrapolated from our experiments applying high-resolution respirometry was that increasing both the concentration and time of exposure to H_2O_2 led to an elevation of what is referred to as “leak respiration”(Figure 6 B).

Leak respiration was measured following the inhibition of ATP synthase by Oligomycin, which induces a state of non-coupling between ATP synthesis and proton cycling.

If the mitochondrial inner membrane (MIM) is completely impermeable to protons, when ATP synthase is inhibited, protons can no longer re-enter the mitochondrial matrix. The matrix becomes progressively depleted of protons, dissipating the chemiosmotic gradient and halting O_2 consumption.

However, if oxygen consumption persists after inhibition with oligomycin, this suggests the presence of proton leakage across the inner mitochondrial membrane towards the matrix. This proton leak fuels protons to complexes I, III and IV, causing the electron transport chain (ETC) to still function at a reduced rate.

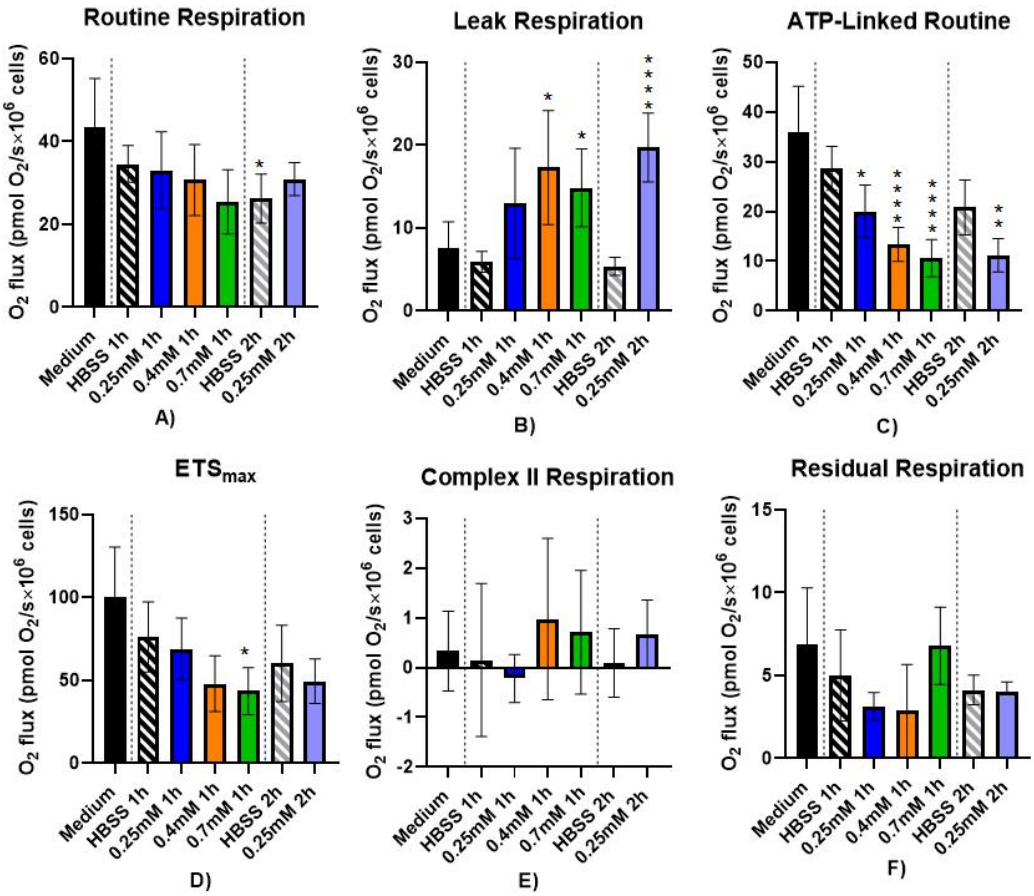

Figure 6: Oxygraphy results expressed as O_2 flux.

Raw O_2 flux values for routine, leak, ETS_{max}, complex II and residual respirations were extracted from Datlab (Appendix Figure A). Values from residual respiration were subtracted from routine, leak, ETS_{max} and complex II respirations values to account for true mitochondrial levels.

A) Routine respiration measurements were obtained by allowing the cells to perform their normal basal respiration in culture medium

B) Leak respiration was assessed after inhibition of ATP synthase using oligomycin

C) ATP-linked respiration was obtained by subtracting Leak respiration values from Routine respiration.

D)ETS_{max} or the maximal ETC capacity was determined after adding an uncoupling agent (FCCP) to the chamber.

E) Respiration from complex II was assessed after inhibition of complex I with rotenone

F) Residual respiration was obtained after inhibition of complex III with antimycine A.

Mean ± SD from five independent experiments for a total of 2 technical replicates per condition per experiment. Conditions include cells incubated in culture medium, HBSS 1h and 2h or H_2O_2 diluted in HBSS (0.25mM 1h and 2h, 0.4mM 1h, 0.7mM 1h).

Normality was respcted for every graphic. A one-way ANOVA was performed followed by a post-hoc Games-Howell's for multipe comparisons.

HBSS control was compared to Medium control. All the H_2O_2-treated samples were compared to the time-equivalent HBSS control.

***Conditions compared to time-equivalent HBSS control**

(*p<0.05; **p<0.01; ***p< 0.001, ****p<0.0001)

Figure 6 shows oxygraphy data expressed as O_2 flux from which residual respiration values were subtracted (Figure 6 F). The values from residual respiration were subtracted from routine, Leak, ETS_{max} and complex II respirations to account for true mitochondrial measurements. Data containing the raw O_2 fluxes is provided in the Appendix section of this thesis (Figure A).

Since O_2 flux can be influenced by a wide array of external factors such as mitochondrial density, cell number and medium composition, pannels from Figure 6 will only be used for analysis of general tendencies amongst the samples.

These results demonstrate that an increase in H_2O_2 is mostly accompanied by an increase in the leak respiration (Figure 6B). As expected, ATP-linked respiration is also affected (Figure 6 C).

The leak and ATP-linked respirations exhibit, respectively, an increase and a decrease in O_2 flux that is dependent on both dose and time of exposure.

Although statistical tests do not show any significant affectation of the other respiratory status, there seems to be a clear tendency for ETS_{max} to drop as the H_2O_2 concentration increases (Figure 6 D).

Finally, the graphic depicting Complex II respiration (Figure 6 E) highlights that the majority of oxygen consumption in the cells is driven by complex I activity rather than complex II.

Data from Figure 6 was further normalized to remove potential confounding factors that could affect the validity of the interpretations (see Figure A2 from Appendix section).

Firstly, raw data was normalized to citrate synthase activity in order to eliminate any variations in mitochondrial content (Raw data/CS).Then, the values obtained after addition of antimicin A (Figure 6 F) were subtracted from Routine, Leak, ETS_{max} and complex II respirations that had been normalized to citrate synthase activity, in order to eliminate the O_2 consumption that was not due to mitochondrial respiration (residual respiration).

Lastly, the values of each respiration state was expressed relative to ETS_{max}, also called Flux control ratio (FCR), to give a proportion of each respiration state (routine, leak, ATP-linked respiration) relative to the maximum respiratory capacity os the sample (ETSmax). FCR is dimensionless, independent of cell count, dry and wet mass, and mitochondrial content of cells and tissues and allows to better comprehend how the different H_2O_2-treatments affect the equilibium between the different respiratory states. For these reasons, results expressed as FCR are more robust. Furthermore, presenting these results as a ratio can be useful to allow comparisons of mitochondrial function across samples.

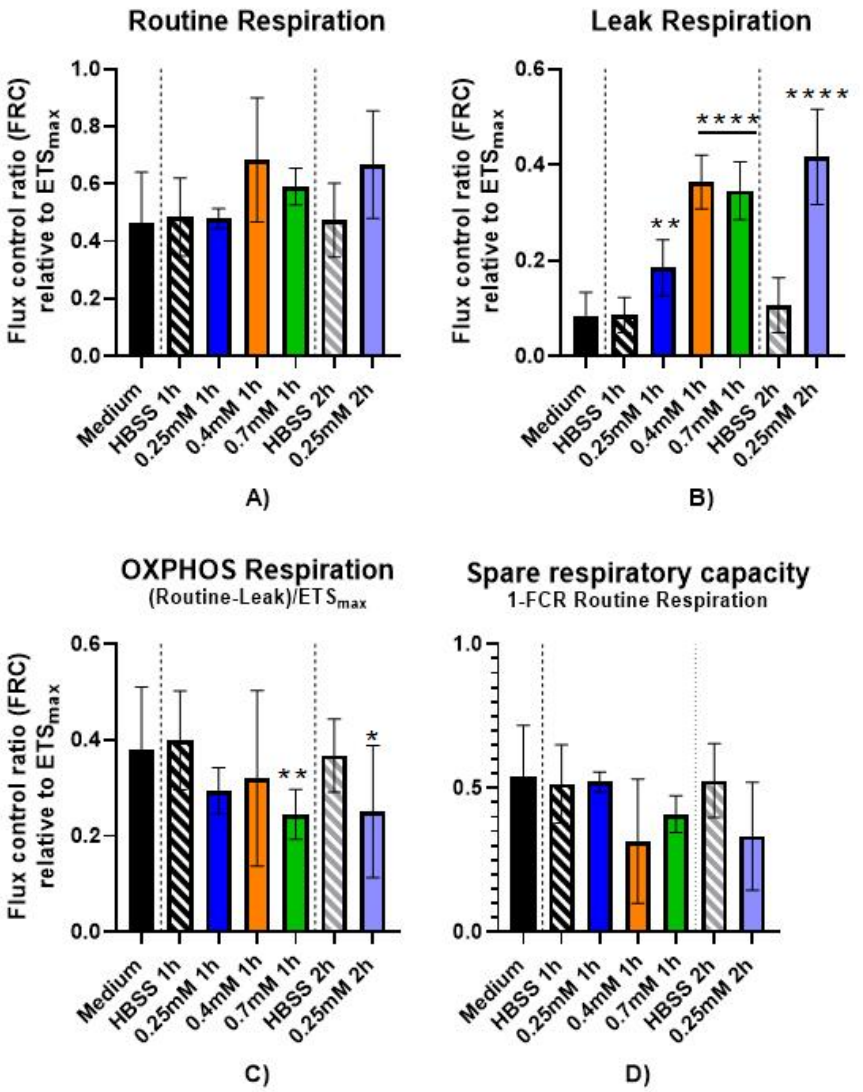

Figure 7: oxygraphy data expressed as Flux Control Ratios (FCR) relative to ETS_{max}.

Raw data from Figure 6 was normalized to citrate synthase activity, corrected for residual respiration and expressed as a rato relative to ETS_{max}.

A) FCR for Routine respiration; B) FCR for Leak respiration; C) FCR for OXPHOS Respiration or ATP-linked routine respiration; D) Spare respiratory capacity

Normality was assessed for each condition but was not respected.

A Kruskal-Wallis test followed by a Dunn's post-hoc test for multiple comparisons was applied.

HBSS 1h and 2h controls were compared to Mi control (Cells in culture medium) to check for a possible effects of the solvant alone. H_2O_2 -treated groups were compared to their respective HBSS time-matched control.

∗Conditions compared to time-equivalent HBSS control

(∗p<0.05; ∗∗p<0.01; ∗∗∗p< 0.001, ∗∗∗∗p<0.0001)

From the results depicted on Figure 7 it was possible to see that the general observations made with the data expressed as O_2 flux was roughly maintained.

Routine respiration (Figure 7 A) showed a slight tendency to increase with the H_2O_2 treatments and with the time of incubation, but nothing that is statistically significant comparing to the respective HBSS controls.

However, for the leak respiration (Figure 7 B), the increase was statistically significant, dose and time-dependent.

Routine respiration includes leak respiration. By subtracting the values from leak respiration from the routine values, we obtain what can be called throughout literature as Net routine, ATP-linked routine or OXPHOS respiration (Figure 7 C). Figure 7 C represents the proportion of the basal respiration that actually leads to ATP synthesis. OXPHOS respiration showed a tendency to decrease, but this is only statistically significant for the highest H_2O_2 concentration and also seemed to be accentuated with the time of incubation (slightly lower for 0.25mM of H_2O_2 for 2h compared to the same concentration for 1h of incubation).

From this data, we could yet calculate the spare respiratory capacity (Figure 7 D), which translates the capacity of the cells to adapt to higher energetic demands or to stress. Cells treated with 0.4mM and 0.7mM of H_2O_2 for 1h seemed to show a slight trend for a lower spare capacity. This tendency also seemed to be amplified by the time of incubation with H_2O_2. While the sample treated with 0.25mM of H_2O_2 for 1h appeared similar to its HBSS time-matched control, the sample treated with 0.25mM for 2h denoted a substantial decrease in the spare capacity even if not statistically significant.

3.2. Citrate synthase activity

We measured the activity of citrate synthase in order to normalize the results from high-resolution respirometry. Citrate synthase activity was itself normalized to total protein content.

From Figure 8 it is possible to say that citrate synthase activity tended to increase with the H_2O_2 treatments. This uprise in the activity seemed to be statistically significant when comparing it to the cells incubated in culture medium, but not when compared to their respective HBSS controls.

These results either suggest that there is a higher mitochondrial density in the H_2O_2-treated cells or that there might be a slight upregulation of the Krebs cycle upon treatment with H_2O_2. If citrate synthase activity is boosted with the H_2O_2-treated samples, it is nor appropriate to normalize HRR results this way, as it can create false negatives. However, as previously shown, both raw oxygraphy data (Figure 6) and data expressed as FCR corrected for residual respiration and normalized to citrate synthase activity (Figure 7) showed roughly the same interpretations (See also Figure A1 and Figure A2 from Appendix).

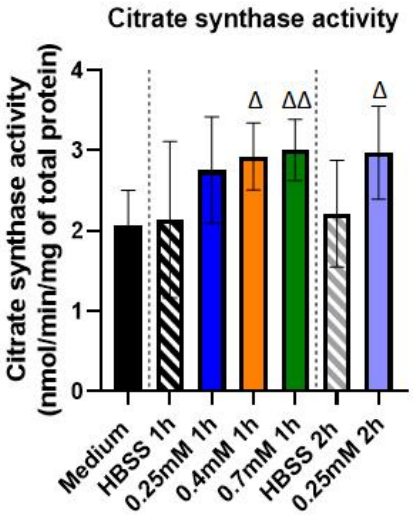

Figure 8: Citrate synthase activity normalized to total protein content.

Tested samples comprise cells incubated in culture medium, HBSS 1h and 2h, and different H_2O_2 concentrations (0.25mM 1h and 2h, 0.4mM 1h, 0.7mM 1h)

Mean ± SD from five independent experiments with 2 technical replicats per condition per experiment.
Normality was verified followed by one way ANOVA and a Games-Howell's multiple compairison test. (p-value=0.0014)
Δ Conditions were compared to the Medium control
(Δ p<0.05; ΔΔ p<0.01; ΔΔΔ p< 0.001, ΔΔΔΔ p<0.0001)

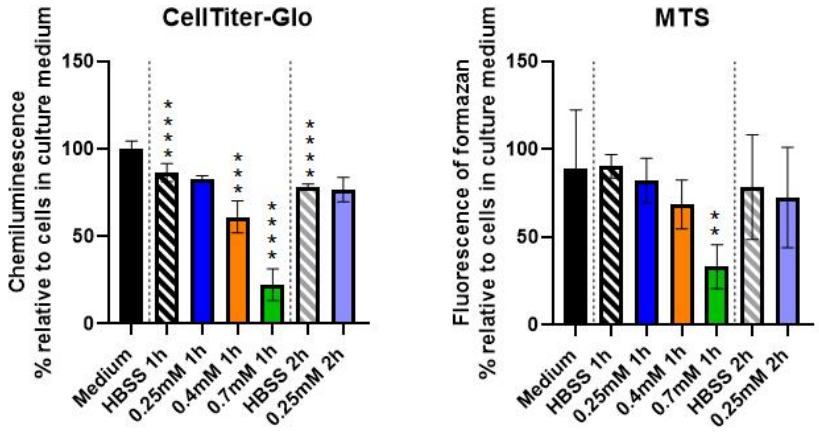

Figure 9: CellTiter-Glo and MTS assays were executed following the same protocol that the one for High-Resolution Respirometry.

Samples tested comprise cells incubated in culture medium, HBSS 1h and 2h, and different H_2O_2 concentrations (0.25mM 1h and 2h, 0.4mM 1h, 0.7mM 1h)

Results are expressed as relative percentage to the cell incubated with culture medium.
Mean ± SD from 3 independent experiments.
Normality was verified for CellTiter-Glo but not for MTS assay.
For CellTiter-Glo a one-way ANOVA was performed (pval<0.0001) followed by a Games-Howell's post-hoc test for multiple comparisons.
For MTS assay a non-parametric Kruskall-Wallis test was performed (pval<0.0001) followed by a Dunn's post-hoc test for multiple comparisons.
HBSS was compared to Medium and H_2O_2 concentrations were compared to their respective time-matched HBSS control.
(∗p<0.05; ∗∗p<0.01; ∗∗∗p< 0.001, ∗∗∗∗p<0.0001

3.3. ROS analysis using H_2DCFda probe

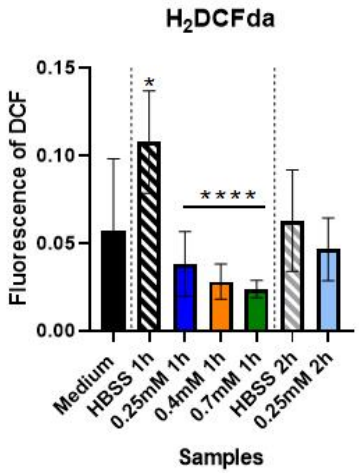

Figure 11: H_2DCFda probe for ROS analysis.

LHCN-M2 cells were incubated with H_2DCFda probe for 30 minutes at 37°C in the dark for ROS levels estimation.

Tested samples comprise cells incubated in culture medium, HBSS 1h and 2h, and different H_2O_2 concentrations (0.25mM 1h and 2h, 0.4mM 1h, 0.7mM 1h)

Mean ± SD from two independent experiments with 6 technical replicates per condition per experiment. Normality was respected. A one-way ANOVA test was performed ($p<0.0001$) followed by a Games-Howell's post-hoc test for multiple comparisons.

HBSS control was compared to Medium control. H_2O_2 conditions compared to time-equivalent HBSS control (* $p<0.05$; ** $p<0.01$; *** $p< 0.001$, **** $p<0.0001$)

When using the H_2DCFda probe to indirectly evaluate intracellular ROS (see introduction and materials & methods for more details).

Incubation of cells with HBSS alone seemed to increase ROS levels, thus the samples treated with increasing H_2O_2 doses have significantly lower intracellular ROS.

Even though statistical tests don't highlight any significant drop in ROS levels in the H_2O_2-treated samples when comparing them to the cells incubated in medium, there is a clear trend for a decrease in ROS levels with an increase in H_2O_2 concentration. These results are somewhat surprising, as we would expect H_2O_2 treatment to lead to an increase in intracellular ROS.

Conclusion
Discussion
Prospectives

1. Discussion & Conclusion

Sarcopenia is an age-related syndrome marked by the progressive loss of skeletal muscle mass and strength. This disorder is associated with a significant decline in the quality of life among affected individuals and generates massive economic burdens on healthcare system, highlighting the urgent need to develop new strategies for its prevention or treatment.

Several well-established *in vivo* models are available to study sarcopenia, including genetically modified models (SOD1 KO mice) and chemically induced models using compounds such as dexamethasone. In contrast, *in vitro* research predominantly relies on three immortalized cell lines: C2C12, L6, LHCN-M2 (Alonso-Puyo J *et al*, 2024). Among these, only LHCN-M2 is human-derived. Although immortalized cell lines provide convenience and reproducibility, they do not fully replicate the biology of sarcopenia, as skeletal muscle cells are post-mitotic and have lost differentiation and proliferation capacities. Primary human muscle cells, obtained through muscle biopsies, offer a more relevant alternative. However, primary cell lines have a limited proliferative capacity and their obtention being through an invasive procedure, not only poses problems for patient compliance but also collecting muscle tissue from individuals suffering from muscle waste is unethical (Alonso- Puyo J *et al*, 2024).

Sarcopenia and other age-related diseases have been widely associated with oxidative stress and mitochondrial dysfunction (Chaudhary MR *et al*, 2023; Ferri E *et al*, 2020; Marzetti E *et al*, 2013).

Numerous studies have demonstrated the impact of exogenous hydrogen peroxide (H_2O_2) on different cell lines (Fu Y *et al*, 2022 (Porcine cells); Anna Laporte et *al*, 2020 (insulin-producing cells); Hack CT *et al*, 2019 (KGN cells); Wang *et al*, 2015 (fish muscle cell line); Fan X *et al*, 2010 (murine myoblasts); McClung JM *et al*, 2008 (murine myoblasts); Li JM *et al*, 2003 (intestinal epithelial cells)).

Additional studies have addressed how exogenous H_2O_2 alters mitochondrial morphology and dynamics (Wang B *et al*, 2024; Garcia I *et al*, 2018; Iqbal S *et al*, 2014; Fan X *et al*, 2010).

However, to our current knowledge, there are no published studies that explicitly describe the effect of an exogenous H_2O_2 treatment on mitochondrial respiration, especially in human muscle cell lines. The only identified article linking LHCN-M2 cells to exogenous H_2O_2 exposure (Mancini A *et al*, 2022) does not investigate its impact on mitochondrial respiration. Our study aims to address part of this gap in research.

Our preliminary experiments using MTS and CellTiter-Glo assays indicate that cells exposed for 1h to several concentrations of H_2O_2 diluted in HBSS reduced, in a dose-dependent manner, the conversion of tetrazolium salt to formazan (Figures 1, 2,3) and as well as decreased ATP production (Figure 5) compared to control conditions with culture medium and HBSS alone. These first results reflected a broad impact in cellular metabolism or in the activity of mitochondrial complexes.

To determine whether these changes reflected true mitochondrial dysfunction rather than a loss of cell viability —which would also reduce signal intensity—we assessed cell death using Sytox Green and Hoechst stainings (Table 1), as well as trypan blue exclusion (Table A1 Appendix) following H_2O_2 treatments. No significant changes were observed between treated (H_2O_2 concentrations) and untreated conditions (Medium or HBSS controls). IncuCyte live-cell imaging (Image 18) confirmed that even at higher H_2O_2 concentrations (1mM), cells remained adherent, indicating a relative preservation of membrane integrity, even if a slight modification of cellular morphology was noticeable.
Together, these results demonstrate that cell viability was largely maintained across the H_2O_2 treated samples, and therefore cannot account for the observed decreases in metabolic readouts (MTS and CellTiter-Glo). Our findings are consistent with previous studies that also used exogenous H_2O_2 treatments (Mizugaki A *et al*, 2022; Fan X *et al*, 2010), although it contrasts with other reports showing increased cytotoxicity under more or less similar conditions (Chen X *et al*, 2023; Xin X *et al*, 2022; Hack CT *et al*, 2019; Wang Q *et al*, 2015; Li JM *et al*, 2003).
Furthermore, the observed decrease in ATP production following different H_2O_2 treatments may explain the increased citrate synthase activity (Figure 8), suggesting a compensatory upregulation of mitochondrial metabolism. This likely reflects an adaptative response aimed at restoring energy balance. Indeed, the activity of the Krebs cycle is tightly regulated by the cellular ATP/ADP ratio. A drop in this ratio accelerates the cycle to refurbish cells with ATP (Arnold PK *et al*, 2023).

When studying mitochondrial respiration in more depth, the statistical tests led in our high resolution respirometry results indicated that leak and ATP-linked respirations were the most affected by the H_2O_2 treatments (Figures 6 B/C and 7 B/C). An increase in leak respiration has already been demonstrated in previous studies involving both endogenous and exogenous H_2O_2 exposure (Yann Voituron *et al*, 2020; Yin J *et al*, 2017).
Membrane integrity and the preservation of cellular compartments are fundamental to maintain homeostasis and represent essential indicators of cellular health. Mitochondria, whose primary role is to produce ATP, are particularly reliant on the structural and functional integrity of their membranes. The electron transport chain (ETC) complexes and ATP synthase are functionally coupled through a proton gradient that is only maintained by the impermeability of the inner mitochondrial membrane to protons, creating a chemiosmotic gradient between the matrix and the intermembrane space which is effectively used by the ATP synthase to produce ATP. Alterations of the inner membrane's structure leads to disruption of the proton gradient and— by extension—impaired ATP production and overall mitochondrial dysfunction. During leak respiration, protons bypass ATP synthase and re-enter the mitochondrial matrix without contributing to ATP production. This process dissipates the proton gradient, thereby reducing the efficiency of oxidative phosphorylation. The resulting decrease in ATP synthesis is

consistent with our findings (Figures 5 and 9) and is further supported by the observed reduction in OXPHOS respiration (Figure 7C).The increase in leak respiration may reflect oxidative damage to mitochondrial lipids, caused by H_2O_2 exposure, which can increase the permeability of the inner mitochondrial membrane (Zheng Yongxin *et al*, 2024; Yin Huiyong *et al*, 2011; Wiswedel I *et al*, 2009). A potential effect of the H_2O_2 on the structural integrity of lipid membranes cannot be excluded, as the LHCN-M2 cells exposed to increasing concentrations of H_2O_2 exhibited altered responses to trypsinization compared to untreated controls (Image A1 Appendix). Following treatment, a subpopulation of cells displayed an elongated, fusiform phenotype that appeared more resistant to detachment and formed cell pellets that were less elastic, more granular, almost sand-like. These observations seem to point towards a broader effect of the hydrogen peroxide on membrane properties (Gaschler MM *et al*, 2018; Catalá A *et al*, 2006).

However, the hypothesis that H_2O_2 affects lipid structure and compromises mitochondrial membrane integrity and impermeability, does not account for the reduced activity of ETC complexes in H_2O_2-treated cells (Figures 4 and 9 MTS assay), nor the general tendency for the ETSmax to decrease (Figure 6 D). In theory, increased membrane permeability would accelerate proton re-entry into the matrix, thereby lowering the proton gradient and stimulating ETC complexes to work at a higher rate to restore it—especially under conditions of ATP depletion. The fact that ETC activity is diminished instead suggests a possible inhibitory effect of H_2O_2 on the respiratory complexes themselves.
The observed decrease in ETC activity, coupled with increased citrate synthase activity and reduced ATP production, may reflect oxidative damage to aconitase. Aconitase, the second enzyme in the krebs cycle, catalyzes the conversion of citrate into isocitrate and contains an iron-sulfur cluster that is especially vulnerable to reactive oxygen species (ROS) (Arnold PK *et al*, 2023). Supporting this hypothesis, a study using an exogenous H_2O_2 treatment on isolated mitochondria from rats' hearts has demonstrated that H_2O_2 selectively inhibits aconitase (Nulton-Persson AC *et al*, 2001; Yan LJ *et al*, 1997), suggesting that ROS-induced inactivation of Krebs cycle enzymes may contribute to the observed metabolic dysfunction. If H_2O_2 damages aconitase, the Krebs cycle is disrupted, leading to a decline in ETC-OXPHOS activity due to lack of cofactors NADH and $FADH_2$. ETC activity would decline (decrease in MTS readouts) and there would be no ATP production (decrease in CellTiter-Glo readouts and in OXPHOS respiration using HRR). Citrate synthase activity, however, may be boosted. As the first enzyme of the Krebs cycle—upstream from aconitase— its activity may increase to compensate for energy shortfalls (Chalifoux O *et al*, 2023). This hypothesis could also explain the observed dose-dependent decrease in both reactive oxygen species (ROS) (Figure 10) and ETSmax capacity (Figure 6 D) following H_2O_2 treatments.We've found contradictory informations in the litterature regarding this hypothesis (Claudia Lennicke et al, 2021;

Lushchak OV *et al*, 2014; Cantu D *et al*, 2011; Matasova LV et *al*, 2008; Tong WH *et al*, 2007). Susana Cadenas (2018) offers an additional perspective by suggesting that ROS levels may decrease under mild mitochondrial uncoupling. Specifically, she describes how a mild dissipation of the protonmotive force (for example increased leak respiration), may lead to ATP production while also decreasing ROS production by decreasing accumulated electrons and probabilities of electron slip.

Taken together, our findings make it difficult to definitively attribute the observed effects to oxidative stress alone. The reduction in ROS levels may also reflect an upregulation of the antioxidant defense systems. Additionally, the observed decrease in ETC activity and ATP production could also result from a cellular shift towards quiescence or senescence, rather than direct mitochondrial impairment (Chandrasekaran A *et al*, 2017; Sasaki M *et al*, 2014; Panieri Emiliano *et al*, 2013; Jianming Duan *et al*, 2005; Andrew C. Lee *et al*, 1999).

Nonetheless, it is appropriate to describe the observed phenotype as mitochondrial distress/ dysfunction or cellular stress, given the clear decrease in ETC activity, increase in leak respiration and collapse of ATP synthesis. These alterations are particularly detrimental in highly metabolic cells such as myoblasts, which rely heavily on aerobic ATP production to sustain their energy demands. Therefore, our results indicate that the exogenous H_2O_2-treatment successfully appears to have induced mitochondrial dysfunction, fulfilling the intended objective of this experimental model.

2. Prospectives

Although our results are extremely encouraging with regards to the effectiveness of H_2O_2 in inducing mitochondrial dysfunction, there are still several ways to further characterize and refine this model. We could, for instance, recur to flow cytometry to evaluate the mitochondrial membrane potential using JC-10 dye or MitoSpy, providing further validation of the observed mitochondrial dysfunction through a collapse of the proton gradient.
Additionally, complementary assays such as mitochondrial swelling tests, cytochrome c release and LDH release could help assess the integrity of mitochondrial membranes.
To strengthen the findings from manual cell death assessments using trypan blue exclusion and Sytox Green, apoptotic and necrotic cell quantification could also be performed using FACS-based assays that allow to differentiate multiple stages of cell-death.

These supplementary approaches are more robust and could help confirm- or refute- that the observed effects are primarily due to a metabolic collapse of mitochondrial function rather than increased cell death over time.

Finally, our results show a decrease in ROS levels with increasing H_2O_2 concentrations (Figure 11). This observation warrants further investigation to determine whether the reduction in ROS is due to enhanced antioxidant systems- such as upregulation of catalase, glutathione peroxidase or myeloperoxidase activity- or whether it reflects a decrease in the activity of deesterases, which makes it so less probe is metabolized and less signal is detected or even if it is due to an inhibition of matricial aconitase activity. This last hypothesis could be explored either by an analysis of aconitase's activity or even by quantifying the NADH/NAD+ ratio or simply by checking if glycolytic enzymes show a higher activity since a mitochondrial dysfunction would mimic an anaerobic situation.

This decrease in ROS production with the H_2O_2 treatment could also be due to a shift in cellular state, such as the onset of mitochondrial fusion, cell death or senescence. β-galactosidase assays combined with cell cycle arrest markers (BrdU, Ki-67) or analysis of senescence-associated secretory phenotype could be used to test this hypothesis.

The first intent of this work was to develop an *in vitro* stress that could effectively induce mitochondrial dysfunction, thereby validating its use as a model for sarcopenia.

In this study, it was chosen to model an acute H_2O_2-induced stress, which contrasts with the chronic oxidative context of sarcopenia. A chronic oxidative stress using H_2O_2 could've been considered using dilutions of glucose oxidase in the culture medium. Glucose oxidase continuously utilizes the glucose and oxygen present in culture medium to produce hydrogen peroxide, thereby mimicking a sustained oxidative environment that may better reflect the conditions observed in age-related muscle degeneration. However, the evaluation of the exact amount of H_2O_2 produced this way would be more complex. One must also not lose sight that all the MitoSir's partners must be able to easily reproduce the model in their own laboratories. Therefore, even if a more pathophysiologically relevant model of sarcopenia using H_2O_2 exists, it would definitely not be suitable for the practical needs of the MitoSir project.

The next step in the MitoSir project, involves exposing the previously H_2O_2-stressed LHCN-M2 cells to primary human muscle-derived stem cells, provided by RevaTis SA., in order to evaluate whether the stem cells can recover, mitigate or reverse the effects of the H_2O_2 treatment—possibly through mitochondrial transfer (Nakhle J *et al*, 2023; Guo Y *et al*, 2020; Paliwal S *et al*, 2018)

Several experimental scenarios could be explored, including pre-stressing the stem cells before co-culture with the LHCN-M2 in order to mimic an aged or compromised micro-environment; assessing

whether the regenerative or protective effects of the stem cells is dependent on the age of the donor; and quantifying mitochondrial dynamics in the stem cells by measuring key markers of fission and fusion both before and after co-culture.

These investigations would provide deeper insights into the mechanisms of potential mitochondrial rescue and the therapeutic relevance of stem cells in models of sarcopenia and other pathologies characterized by oxidative stress or mitochondrial dysfunction.

References

Alonso-Puyo J, Izagirre-Fernandez O, Crende O, Valdivia A, García-Gallastegui P, Sanz B. Experimental models as a tool for research on sarcopenia: A narrative review. Ageing Res Rev. 2024 Nov;101:102534. doi: 10.1016/j.arr.2024.102534.

Anderson S, Bankier AT, Barrell BG, de Bruijn MH, Coulson AR, Drouin J, Eperon IC, Nierlich DP, Roe BA, Sanger F, Schreier PH, Smith AJ, Staden R, Young IG. Sequence and organization of the human mitochondrial genome. Nature. 1981 Apr 9;290(5806):457-65. doi: 10.1038/290457a0.

Andrew C. Lee, Brett E. Fenster, Hideki Ito, Kazuyo Takeda, Nancy S. Bae, Tazuko Hirai, Zu-Xi Yu, Victor J. Ferrans, Bruce H. Howard, Toren Finkel, Ras Proteins Induce Senescence by Altering the Intracellular Levels of Reactive Oxygen Species*, Journal of Biological Chemistry, Volume 274, Issue 12,1999, Pages 7936-7940, ISSN 0021-9258,DOI:10.1074/jbc.274.12.7936.

Anna Laporte, Stephan Lortz, Christina Schaal, Sigurd Lenzen, Matthias Elsner, Hydrogen peroxide permeability of cellular membranes in insulin-producing cells, Biochimica et Biophysica Acta (BBA) - Biomembranes, Volume 1862, Issue 2, 2020, 183096, ISSN 0005-2736, DOI: 10.1016/j.bbamem.2019.183096.

Arnold PK, Finley LWS. Regulation and function of the mammalian tricarboxylic acid cycle. J Biol Chem. 2023 Feb;299(2):102838. doi: 10.1016/j.jbc.2022.102838. Epub 2022 Dec 26. PMID: 36581208; PMCID: PMC9871338.

Ayub A, Cheong YK, Castro JC, Cumberlege O, Chrysanthou A. Use of Hydrogen Peroxide Vapour for Microbiological Disinfection in Hospital Environments: A Review. Bioengineering (Basel). 2024 Feb 22;11(3):205. doi: 10.3390/bioengineering11030205.

Baker JS, McCormick MC, Robergs RA. Interaction among Skeletal Muscle Metabolic Energy Systems during Intense Exercise. J Nutr Metab. 2010;2010:905612. doi: 10.1155/2010/905612.

Bienert GP, Chaumont F. Aquaporin-facilitated transmembrane diffusion of hydrogen peroxide. Biochim Biophys Acta. 2014 May;1840(5):1596-604. doi: 10.1016/j.bbagen.2013.09.017.

Bienert GP, Møller AL, Kristiansen KA, Schulz A, Møller IM, Schjoerring JK, Jahn TP. Specific aquaporins facilitate the diffusion of hydrogen peroxide across membranes. J Biol Chem. 2007 Jan 12;282(2):1183-92. doi: 10.1074/jbc.M603761200.

Bienert GP, Schjoerring JK, Jahn TP. Membrane transport of hydrogen peroxide. Biochim Biophys Acta. 2006 Aug;1758(8):994-1003. doi:10.1016/j.bbamem.2006.02.015.

Cantu D, Fulton RE, Drechsel DA, Patel M. Mitochondrial aconitase knockdown attenuates paraquat-induced dopaminergic cell death via decreased cellular metabolism and release of iron and H_2O_2. J Neurochem. 2011 Jul;118(1):79-92. doi: 10.1111/j.1471-4159.2011.07290.x.

Catalá A. An overview of lipid peroxidation with emphasis in outer segments of photoreceptors and the chemiluminescence assay. Int J Biochem Cell Biol. 2006;38(9):1482-95. doi:10.1016/j.biocel.2006.02.010.

Chalifoux O, Faerman B, Mailloux RJ. Mitochondrial hydrogen peroxide production by pyruvate dehydrogenase and α-ketoglutarate dehydrogenase in oxidative eustress and oxidative distress. J Biol Chem. 2023 Dec;299(12):105399. doi: 10.1016/j.jbc.2023.105399.

Chandrasekaran A, Idelchik MDPS, Melendez JA. Redox control of senescence and age-related disease. Redox Biol. 2017 Apr;11:91-102. doi: 10.1016/j.redox.2016.11.005.

Chaudhary MR, Chaudhary S, Sharma Y, Singh TA, Mishra AK, Sharma S, Mehdi MM. Aging, oxidative stress and degenerative diseases: mechanisms, complications and emerging therapeutic strategies. Biogerontology. 2023 Oct;24(5):609-662. doi: 10.1007/s10522-023-10050-1.

Chen X, Tzekov R, Su M, Zhu Y, Han A, Li W. Hydrogen peroxide-induced oxidative damage and protective role of peroxiredoxin 6 protein via EGFR/ERK signaling pathway in RPE cells. Front Aging Neurosci. 2023 Jul 17;15:1169211. doi: 10.3389/fnagi.2023.1169211.

Claudia Lennicke, Helena M. Cochemé, Redox metabolism: ROS as specific molecular regulators of cell signaling and function, Molecular Cell, Volume 81, Issue 18, 2021, Pages 3691-3707, ISSN 1097-2765, DOI: 10.1016/j.molcel.2021.08.018.

Cogliati S, Cabrera-Alarcón JL, Enriquez JA. Regulation and functional role of the electron transport chain supercomplexes. Biochem Soc Trans. 2021 Dec 17;49(6):2655-2668. doi: 10.1042/BST20210460.

Colina-Tenorio L, Horten P, Pfanner N, Rampelt H. Shaping the mitochondrial inner membrane in health and disease. J Intern Med. 2020 Jun;287(6):645-664. doi: 10.1111/joim.13031.

Damluji AA, Alfaraidhy M, AlHajri N, Rohant NN, Kumar M, Al Malouf C, Bahrainy S, Ji Kwak M, Batchelor WB, Forman DE, Rich MW, Kirkpatrick J, Krishnaswami A, Alexander KP, Gerstenblith G, Cawthon P, deFilippi CR, Goyal P. Sarcopenia and Cardiovascular Diseases. Circulation. 2023 May 16;147(20):1534-1553. doi: 10.1161/CIRCULATIONAHA.123.064071.

Di Marzo N, Chisci E, Giovannoni R. The Role of Hydrogen Peroxide in Redox-Dependent Signaling: Homeostatic and Pathological Responses in Mammalian Cells. Cells. 2018 Oct 4;7(10):156. doi: 10.3390/cells7100156. PMID: 30287799; PMCID: PMC6211135.

Divakaruni AS, Brand MD. The regulation and physiology of mitochondrial proton leak. Physiology (Bethesda). 2011 Jun;26(3):192-205. doi:10.1152/physiol.00046.2010.

Ege T, Tao L, North BJ. The Role of Molecular and Cellular Aging Pathways on Age-Related Hearing Loss. Int J Mol Sci. 2024 Sep 7;25(17):9705. doi: 10.3390/ijms25179705.

Fan X, Hussien R, Brooks GA. H2O2-induced mitochondrial fragmentation in C2C12 myocytes. Free Radic Biol Med. 2010 Dec 1;49(11):1646-54. doi: 10.1016/j.freeradbiomed.2010.08.024.

Fernández-Moreno M, Hermida-Gómez T, Gallardo ME, Dalmao-Fernández A, Rego-Pérez I, Garesse R, Blanco FJ. Generating Rho-0 Cells Using Mesenchymal Stem Cell Lines. PLoS One. 2016 Oct 20;11(10):e0164199. doi: 10.1371/journal.pone.0164199.

Ferri E, Marzetti E, Calvani R, Picca A, Cesari M, Arosio B. Role of Age-Related Mitochondrial Dysfunction in Sarcopenia. Int J Mol Sci. 2020 Jul 23;21(15):5236. doi: 10.3390/ijms21155236.

Forman HJ. Use and abuse of exogenous H2O2 in studies of signal transduction. Free Radic Biol Med. 2007 Apr 1;42(7):926-32. doi:10.1016/j.freeradbiomed.2007.01.011.

Frédéric N. Daussin, Eric Boulanger, Steve Lancel,From mitochondria to sarcopenia: Role of inflammaging and RAGE-ligand axis implication,Experimental Gerontology,Volume 146,2021,111247,ISSN 0531-5565,DOI:10.1016/j.exger.2021.111247.

Fu Y, Chen Y, Jin Z, Gao H, Song G, Wang Q, Xu K. Melatonin Alleviates Oxidative Stress Induced by H2O2 in Porcine Trophectoderm Cells. Antioxidants (Basel). 2022 May 25;11(6):1047. doi: 10.3390/antiox11061047. PMID: 35739944; PMCID: PMC9219737.

Garcia I, Innis-Whitehouse W, Lopez A, Keniry M, Gilkerson R. Oxidative insults disrupt OPA1-mediated mitochondrial dynamics in cultured mammalian cells. Redox Rep. 2018 Dec;23(1):160-167. doi: 10.1080/13510002.2018.1492766.

Gaschler MM, Andia AA, Liu H, Csuka JM, Hurlocker B, Vaiana CA, Heindel DW, Zuckerman DS, Bos PH, Reznik E, Ye LF, Tyurina YY, Lin AJ, Shchepinov MS, Chan AY, Peguero-Pereira E, Fomich MA, Daniels JD, Bekish AV, Shmanai VV, Kagan VE, Mahal LK, Woerpel KA, Stockwell BR. FINO2 initiates ferroptosis through GPX4 inactivation and iron oxidation. Nat Chem Biol. 2018 May;14(5):507-515. doi: 10.1038/s41589-018-0031-6.

Gisela Storz, James A Imlayt, Oxidative stress, Current Opinion in Microbiology, Volume 2, Issue 2, 1999, Pages 188-194, ISSN 1369-5274, DOI:10.1016/S1369-5274(99)80033-2.

Greco M, Villani G, Mazzucchelli F, Bresolin N, Papa S, Attardi G. Marked aging-related decline in efficiency of oxidative phosphorylation in human skin fibroblasts. FASEB J. 2003 Sep;17(12):1706-8. doi: 10.1096/fj.02-1009fje.

Guo Y, Chi X, Wang Y, Heng BC, Wei Y, Zhang X, Zhao H, Yin Y, Deng X. Mitochondria transfer enhances proliferation, migration, and osteogenic differentiation of bone marrow mesenchymal stem cell and promotes bone defect healing. Stem Cell Res Ther. 2020 Jun 25;11(1):245. doi: 10.1186/s13287-020-01704-9.

Hack CT, Buck T, Bagnjuk K, Eubler K, Kunz L, Mayr D, Mayerhofer A. A Role for H2O2 and TRPM2 in the Induction of Cell Death: Studies in KGN Cells. Antioxidants (Basel). 2019 Oct 29;8(11):518. doi: 10.3390/antiox8110518.

Holloway GP, Holwerda AM, Miotto PM, Dirks ML, Verdijk LB, van Loon LJC. Age-Associated Impairments in Mitochondrial ADP Sensitivity Contribute to Redox Stress in Senescent Human Skeletal Muscle. Cell Rep. 2018 Mar 13;22(11):2837-2848. doi: 10.1016/j.celrep.2018.02.069. PMID: 29539414.

Hütter, E & Unterluggauer, Hermann & Garedew, A & Jansen-Dürr, P & Gnaiger, Erich. (2006). High-resolution respirometry–a modern tool in aging research. Experimental gerontology. 41. 103-9. 10.1016/j.exger.2005.09.011.

Iqbal S, Hood DA. Oxidative stress-induced mitochondrial fragmentation and movement in skeletal muscle myoblasts. Am J Physiol Cell Physiol. 2014 Jun 15;306(12):C1176-83. doi:10.1152/ajpcell.00017.2014.

Jianming Duan, Jianping Duan, Zongyu Zhang, Tanjun Tong, Irreversible cellular senescence induced by prolonged exposure to H2O2 involves DNA-damage-and-repair genes and telomere shortening, The International Journal of Biochemistry & Cell Biology, Volume 37, Issue 7,2005,Pages 1407-1420,ISSN 1357-2725, DOI: 10.1016/j.biocel.2005.01.010.

Kamarulzaman, N.T., Makpol, S. The link between Mitochondria and Sarcopenia. *J Physiol Biochem* 81, 1–20 (2025). https://doi.org/10.1007/s13105-024-01062-7.

Katori R, Hayashi R, Kobayashi Y, Kobayashi E, Nishida K. (2016). Ebselen Preserves Tissue-Engineered Cell Sheets and their Stem Cells in Hypothermic Conditions. Scientific Reports. 6. 38987. DOI: 10.1038/srep38987.

Kurnat-Thoma EL, Murray MT, Juneau P. Frailty and Determinants of Health Among Older Adults in the United States 2011-2016. J Aging Health. 2022 Mar;34(2):233-244. doi: 10.1177/08982643211040706.

Lena A, Anker MS, Springer J. Muscle Wasting and Sarcopenia in Heart Failure-The Current State of Science. Int J Mol Sci. 2020 Sep 8;21(18):6549. doi: 10.3390/ijms21186549.

Liang Z, Zhang T, Liu H, Li Z, Peng L, Wang C, Wang T. Inflammaging: The ground for sarcopenia? Exp Gerontol. 2022 Oct 15;168:111931. doi: 10.1016/j.exger.2022.111931.

Li JM, Zhou H, Cai Q, Xiao GX. Role of mitochondrial dysfunction in hydrogen peroxide-induced apoptosis of intestinal epithelial cells. World J Gastroenterol. 2003 Mar;9(3):562-7. doi: 10.3748/wjg.v9.i3.562.

Liu S, Qiu Y, Xiang R, Huang P. Characterization of H2O2-Induced Alterations in Global Transcription of mRNA and lncRNA. Antioxidants (Basel). 2022 Mar 3;11(3):495. doi: 10.3390/antiox11030495.

López-Otín C, Blasco MA, Partridge L, Serrano M, Kroemer G. Hallmarks of aging: An expanding universe. Cell. 2023 Jan 19;186(2):243-278. doi: 10.1016/j.cell.2022.11.001.

Luciani, A., Denley, M.C.S., Govers, L.P. *et al.* Mitochondrial disease, mitophagy, and cellular distress in methylmalonic acidemia. *Cell. Mol. Life Sci.* 78, 6851–6867 (2021). doi: 10.1007/s00018-021-03934-3.

Lushchak OV, Piroddi M, Galli F, Lushchak VI. Aconitase post-translational modification as a key in linkage between Krebs cycle, iron homeostasis, redox signaling, and metabolism of reactive oxygen species. Redox Rep. 2014 Jan;19(1):8-15. doi: 10.1179/1351000213Y.0000000073.

Mancini A, Vitucci D, Labruna G, Orrù S, Buono P. Effects of Different Types of Chronic Training on Bioenergetic Profile and Reactive Oxygen Species Production in LHCN-M2 Human Myoblast Cells. Int J Mol Sci. 2022 Jul 6;23(14):7491. doi: 10.3390/ijms23147491.

Marzetti E, Calvani R, Cesari M, Buford TW, Lorenzi M, Behnke BJ, Leeuwenburgh C. Mitochondrial dysfunction and sarcopenia of aging: from signaling pathways to clinical trials. Int J Biochem Cell Biol. 2013 Oct;45(10):2288-301. doi: 10.1016/j.biocel.2013.06.024.

Matasova LV, Popova TN. Aconitate hydratase of mammals under oxidative stress. Biochemistry (Mosc). 2008 Sep;73(9):957-64. doi: 10.1134/s0006297908090010.

McClung JM, Judge AR, Talbert EE, Powers SK. Calpain-1 is required for hydrogen peroxide-induced myotube atrophy. Am J Physiol Cell Physiol. 2009 Feb;296(2):C363-71. doi: 10.1152/ajpcell.00497.2008.

Mizugaki A., Kato H., Takeda T. *et al.* Cystine reduces mitochondrial dysfunction in C2C12 myotubes under moderate oxidative stress induced by H2O2. *Amino Acids* 54, 1203–1213 (2022). doi: 10.1007/s00726-022-03176-y.

Monireh Dashty, A quick look at biochemistry: Carbohydrate metabolism,Clinical Biochemistry,Volume 46, Issue 15,2013, Pages 1339-1352, ISSN 0009-9120,Doi: 10.1016/j.clinbiochem.2013.04.027.

Nakhle J, Khattar K, Özkan T, Boughlita A, Abba Moussa D, Darlix A, Lorcy F, Rigau V, Bauchet L, Gerbal-Chaloin S, Daujat-Chavanieu M, Bellvert F, Turchi L, Virolle T, Hugnot JP, Buisine N, Galloni M, Dardalhon V, Rodriguez AM, Vignais ML. Mitochondria Transfer from Mesenchymal Stem Cells Confers Chemoresistance to Glioblastoma Stem Cells through Metabolic Rewiring. Cancer Res Commun. 2023 Jun 14;3(6):1041-1056. doi: 10.1158/2767-9764.CRC-23-0144.

Nova, Z.; Skovierova, H.; Strnadel, J.; Halasova, E.; Calkovska, A. Short-Term versus Long-Term Culture of A549 Cells for Evaluating the Effects of Lipopolysaccharide on Oxidative Stress, Surfactant Proteins and Cathelicidin LL-37. *Int. J. Mol. Sci.* 2020, *21*, 1148. https://doi.org/10.3390/ijms21031148

Nulton-Persson AC, Szweda LI. Modulation of mitochondrial function by hydrogen peroxide. J Biol Chem. 2001 Jun 29;276(26):23357-61. doi: 10.1074/jbc.M100320200.

Paliwal, S., Chaudhuri, R., Agrawal, A. *et al.* Human tissue-specific MSCs demonstrate differential mitochondria transfer abilities that may determine their regenerative abilities. *Stem Cell Res Ther* 9, 298 (2018). DOI: 10.1186/s13287-018-1012-0

Panieri, Emiliano & Gogvadze, Vladimir & Norberg, Erik & Venkatesh, Rithika & Orrenius, Sten & Zhivotovsky, Boris. (2013). Reactive Oxygen Species generated in different compartments induce cell death, survival or senescence.. Free radical biology & medicine. 57. 10.1016/j.freeradbiomed.2012.12.024.

Panov AV, Dikalov SI. Cardiolipin, Perhydroxyl Radicals, and Lipid Peroxidation in Mitochondrial Dysfunctions and Aging. Oxid Med Cell Longev. 2020 Sep 8;2020:1323028. doi: 10.1155/2020/1323028.

Park SS, Kwon ES, Kwon KS. Molecular mechanisms and therapeutic interventions in sarcopenia. Osteoporos Sarcopenia. 2017 Sep;3(3):117-122. doi:10.1016/j.afos.2017.08.098.

Pesta D, Gnaiger E. High-resolution respirometry: OXPHOS protocols for human cells and permeabilized fibers from small biopsies of human muscle. Methods Mol Biol. 2012;810:25-58. doi: 10.1007/978-1-61779-382-0_3.

González-Gualda E, Baker AG, Fruk L, Muñoz-Espín D. A guide to assessing cellular senescence in vitro and in vivo. FEBS J. 2021 Jan;288(1):56-80. doi:10.1111/febs.15570.

Picca A, Calvani R. Molecular Mechanism and Pathogenesis of Sarcopenia: An Overview. Int J Mol Sci. 2021 Mar 16;22(6):3032. doi: 10.3390/ijms22063032.

Porter C, Hurren NM, Cotter MV, Bhattarai N, Reidy PT, Dillon EL, Durham WJ, Tuvdendorj D, Sheffield-Moore M, Volpi E, Sidossis LS, Rasmussen BB, Børsheim E. Mitochondrial respiratory capacity and coupling control decline with age in human skeletal muscle. Am J Physiol Endocrinol Metab. 2015 Aug 1;309(3):E224-32. doi: 10.1152/ajpendo.00125.2015. Epub 2015 Jun 2. Erratum in: Am J Physiol Endocrinol Metab. 2015 Nov 15;309(10):E884. doi: 10.1152/ajpendo.zh1-7407-corr.2015.

Pye D, Kyriakouli DS, Taylor GA, Johnson R, Elstner M, Meunier B, Chrzanowska-Lightowlers ZM, Taylor RW, Turnbull DM, Lightowlers RN. Production of transmitochondrial cybrids containing naturally occurring pathogenic mtDNA variants. Nucleic Acids Res. 2006 Aug 2;34(13):e95. doi: 10.1093/nar/gkl516.

Sasaki M, Kajiya H, Ozeki S, Okabe K, Ikebe T. Reactive oxygen species promotes cellular senescence in normal human epidermal keratinocytes through epigenetic regulation of p16(INK4a.). Biochem Biophys Res Commun. 2014 Sep 26;452(3):622-8. doi: 10.1016/j.bbrc.2014.08.123. Epub 2014 Aug 30. Erratum in: Biochem Biophys Res Commun. 2018 Oct 28;505(2):634-635. doi: 10.1016/j.bbrc.2018.09.063.

Siu PM, Wang Y, Alway SE. Apoptotic signaling induced by H2O2-mediated oxidative stress in differentiated C2C12 myotubes. Life Sci. 2009 Mar 27;84(13-14):468-81. doi: 10.1016/j.lfs.2009.01.014.

Shen X, Sun P, Zhang H, Yang H. Mitochondrial quality control in the brain: The physiological and pathological roles. Front Neurosci. 2022 Dec 12;16:1075141. doi:10.3389/fnins.2022.1075141.

Short KR, Bigelow ML, Kahl J, Singh R, Coenen-Schimke J, Raghavakaimal S, Nair KS. Decline in skeletal muscle mitochondrial function with aging in humans. Proc Natl Acad Sci U S A. 2005 Apr 12;102(15):5618-23. doi: 10.1073/pnas.0501559102.

Strauss M, Hofhaus G, Schröder RR, Kühlbrandt W. Dimer ribbons of ATP synthase shape the inner mitochondrial membrane. EMBO J. 2008 Apr 9;27(7):1154-60. doi: 10.1038/emboj.2008.35.

Susana Cadenas, Mitochondrial uncoupling, ROS generation and cardioprotection, Biochimica et Biophysica Acta (BBA) - Bioenergetics, Volume 1859, Issue 9, 2018, Pages 940-950, ISSN 0005-2728, DOI: 10.1016/j.bbabio.2018.05.019.

Tong WH., Rouault T.A. Metabolic regulation of citrate and iron by aconitases: role of iron–sulfur cluster biogenesis. *Biometals* 20, 549–564 (2007). DOI:10.1007/s10534-006-9047-6

Tonkonogi M, Fernström M, Walsh B, Ji LL, Rooyackers O, Hammarqvist F, Wernerman J, Sahlin K. Reduced oxidative power but unchanged antioxidative capacity in skeletal muscle from aged humans. Pflugers Arch. 2003 May;446(2):261-9. doi: 10.1007/s00424-003-1044-9.

Visavadiya NP, Rossiter HB, Khamoui AV. Distinct glycolytic pathway regulation in liver, tumour and skeletal muscle of mice with cancer cachexia. Cell Biochem Funct. 2021 Aug;39(6):802-812. doi: 10.1002/cbf.3652.

Wang B., Xu H., Shang S., Liu L., Sun C., & Du W. (2024). Irisin improves ROS- induced mitohormesis imbalance in H9c2 cells. Molecular Medicine Reports, 30, 240. DOI:10.3892/mmr.2024.13364.

Wang, Qiuju & Ju, Xue & Chen, Yuke & Dong, Xiaoqing & Luo, Sha & Liu, Hongjian & Zhang, Dongming. (2015). L-carnitine exerts a cytoprotective effect against H2O2-induced oxidative stress in the fathead minnow muscle cell line. Aquaculture Research. 48. DOI:10.1111/are.12937.

Wang Q, Yuan Y, Liu J, Li C, Jiang X. The role of mitochondria in aging, cell death, and tumor immunity. Front Immunol. 2024 Dec 23;15:1520072. doi: 10.3389/fimmu.2024.1520072.

Wang T. Searching for the link between inflammaging and sarcopenia. Ageing Res Rev. 2022 May;77:101611. doi: 10.1016/j.arr.2022.101611.

Wiswedel I. F(2)-isoprostanes: sensitive biomarkers of oxidative stress in vitro and in vivo: a gas chromatography-mass spectrometric approach. Methods Mol Biol. 2009;580:3-16. doi: 10.1007/978-1-60761-325-1_1.

Xin, X., Gong, T. & Hong, Y. Hydrogen peroxide initiates oxidative stress and proteomic alterations in meningothelial cells. *Sci Rep* 12, 14519 (2022). DOI:10.1038/s41598-022-18548-3.

Yan LJ, Levine RL, Sohal RS. Oxidative damage during aging targets mitochondrial aconitase. Proc Natl Acad Sci U S A. 1997 Oct 14;94(21):11168-72. doi: 10.1073/pnas.94.21.11168. Erratum in: Proc Natl Acad Sci U S A 1998 Feb 17;95(4):1968.

Yann Voituron, Mélanie Boël, Damien Roussel, Mitochondrial threshold for H2O2 release in skeletal muscle of mammals, Mitochondrion, Volume 54, 2020, Pages 85-91, ISSN 1567-7249,doi: 10.1016/j.mito.2020.07.005.

Yin, Huiyong & Zhu, Mingjiang. (2012). Free radical oxidation of cardiolipin: Chemical mechanisms, detection and implication in apoptosis, mitochondrial dysfunction and human diseases. Free radical research. 46. 959-74. DOI:10.3109/10715762.2012.676642.

Yin J, Wu M, Li Y, Ren W, Xiao H, Chen S, Li C, Tan B, Ni H, Xiong X, Zhang Y, Huang X, Fang R, Li T, Yin Y. Toxicity assessment of hydrogen peroxide on Toll-like receptor system, apoptosis, and mitochondrial respiration in piglets and IPEC-J2 cells. Oncotarget 2017 Jan 10;8(2):3124-3131, DOI:10.18632/oncotarget.13844.

Zheng, Yongxin & Sun, Junlu & Luo, Zhiting & Li, Yimin & Huang, Yongbo. (2024). Emerging mechanisms of lipid peroxidation in regulated cell death and its physiological implications. Cell Death & Disease. 15. 10.1038/s41419-024-07244-x.

Other references:

(Biologie Anatomie Physiologie, Nicole Menche, 9th edition, ISBN: 978-2-294-77396-9)

Appendix

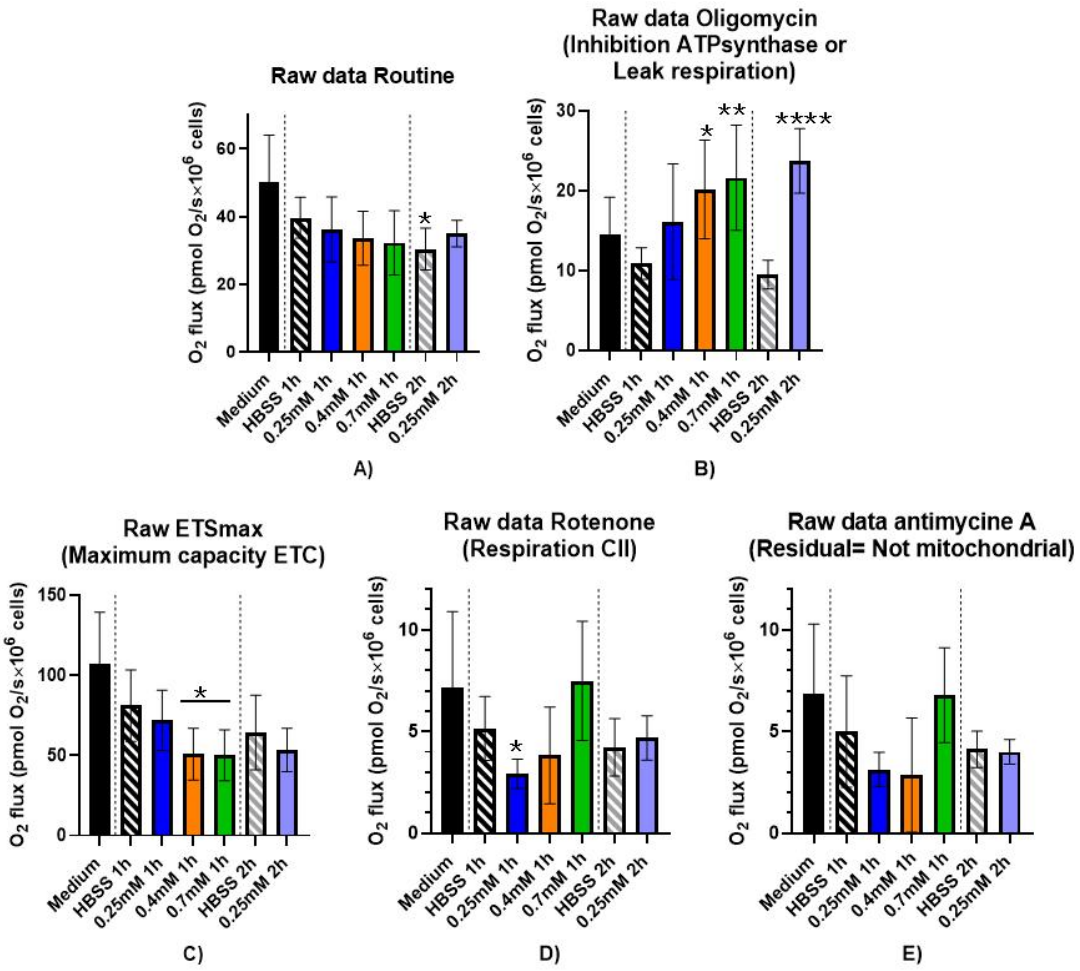

Figure A1: Raw O2 flux data extracted from DatLab Software

A) Routine respiration measurements were obtained by allowing the cells to perform their normal basal respiration in culture medium

B) Leak respiration was assessed after inhibition of ATP synthase using oligomycin

C)ETS_{max} or the maximal ETC capacity was determined after adding an uncoupling agent (FCCP) to the chamber.

D)Respiration from complex II was assessed after inhibition of complex I with rotenone

E)Residual respiration was obtained after inhibition of complex III with antimycine A.

Mean ± SD from five independent experiments for a total of 2 technical replicates per condition per experiment. Conditions include cells incubated in culture medium, HBSS 1h and 2h or H_2O_2 diluted in HBSS (0.25mM 1h and 2h, 0.4mM 1h, 0.7mM 1h).

Normality was respected for every graphic. A one-way ANOVA was performed followed by a post-hoc Games-Howell's for multiple comparisons.

HBSS control was compared to Medium control. All the H_2O_2-treated samples were compared to the time-equivalent HBSS control.

***Conditions compared to time-equivalent HBSS control**

(*p<0.05; **p<0.01; ***p< 0.001, ****p<0.0001)

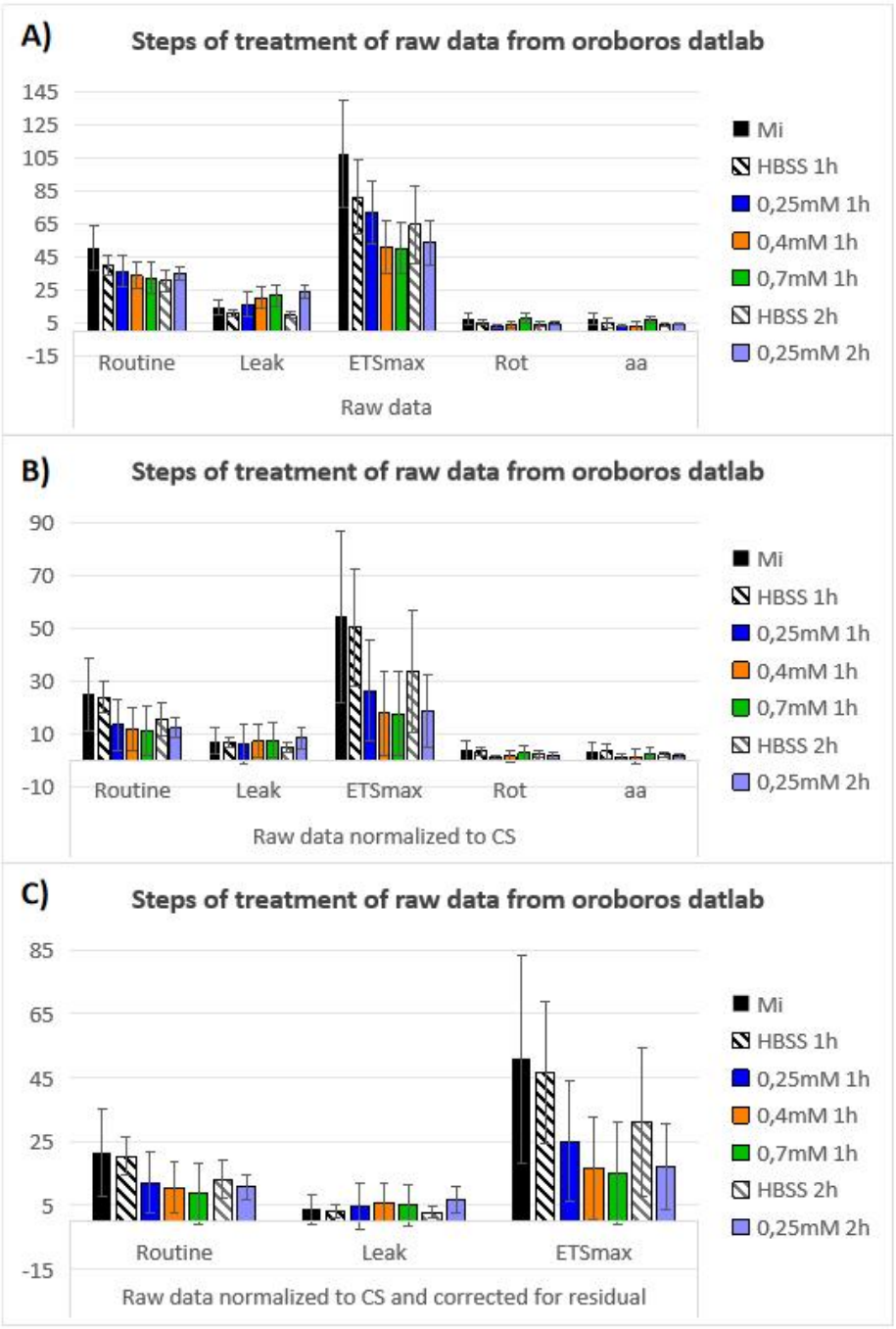

Figure A2: Representation of every normalization step to the Raw O_2 flux from Figure A (Appendix)

A) Raw O_2 flux (Same data as Figure A)

B) Raw O2 flux data was normalized to citrate synthase activity

C)The data normalized to citrate synthase activity was corrected for residual respiration by subtracting O2 flux values after addition of antimycin a (aa).

Condition	Cell number by flask (million)	% Cell mortality (Mean ± SD)
Milieu	5.1 ± 0.5	0.6 ± 0.6
HBSS (1h)	4.8 ± 0.5	1.7 ± 1.5
H_2O_2 (0.25 mM) (1h)	4.3 ± 0.3	1.3 ± 1.5
H_2O_2 (0.4 mM) (1h)	4.6 ± 0.5	2.1 ± 0.8
H_2O_2 (0.7 mM) (1h)	4.6 ± 0.5	3.2 ± 0.3
HBSS (2h)	5.4 ± 0.4	0.5 ± 0.8
H_2O_2 (0.25 mM) (2h)	4.7 ± 0.2	1.3 ± 1.0

Table A1: Cell number and mortality of LHCN-M2 cells after their exposure (1h or 2h) or not (Milieu and HBSS) to several H_2O_2 concentrations.
Cells were detached from the T75 flasks with trypsin and cell pellet was resuspended in 1ml medium. Trypan blue exclusion test was used to assess cell mortality throughout the oxygraphy samples.
Samples comprise cells incubated in culture medium, HBSS 1h and 2h, and different H_2O_2 concentrations (0.25mM 1h and 2h, 0.4mM 1h, 0.7mM 1h);
Normality was verified.
For cell mortality, normality was not met, a non-parametric Kruskall-Wallis test was performed (pval=0.0917) followed by a Dunn's post-hoc test for multiple comparisons.
HBSS was compared to Medium and H_2O_2 concentrations were compared to their respective time-matched HBSS control. Significant p-values were found
Mean ± SD from 3 independent experiments.

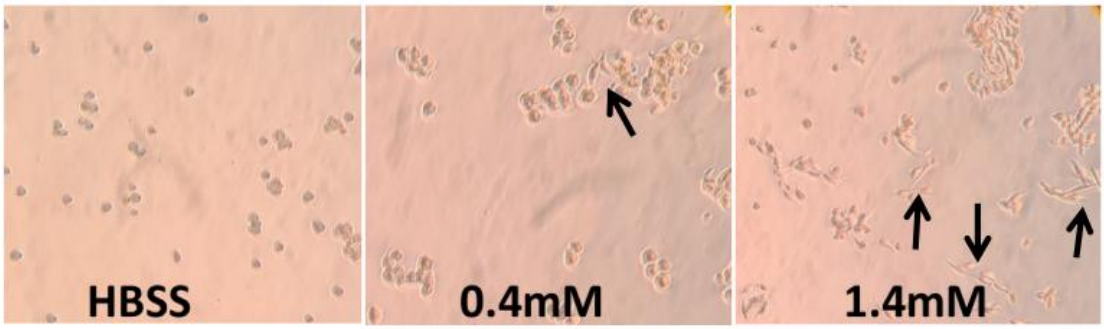

Image A1: Photos taken of LHCN-M2 cells after 5 minutes with trypsin.
Cells treated with only HBSS presented a well rounded shape, while cells treated with H_2O_2 showed heterogenous morphologies. There was the apparition of more fusiform cells with the H_2O_2 concentration. G: 10x